Linking Titan's properties to its formation conditions

A large NH_3 inventory in Titan's building blocks supports the presence of a subsurface ocean

C.N. Immerzeel

Technische Universiteit Delft

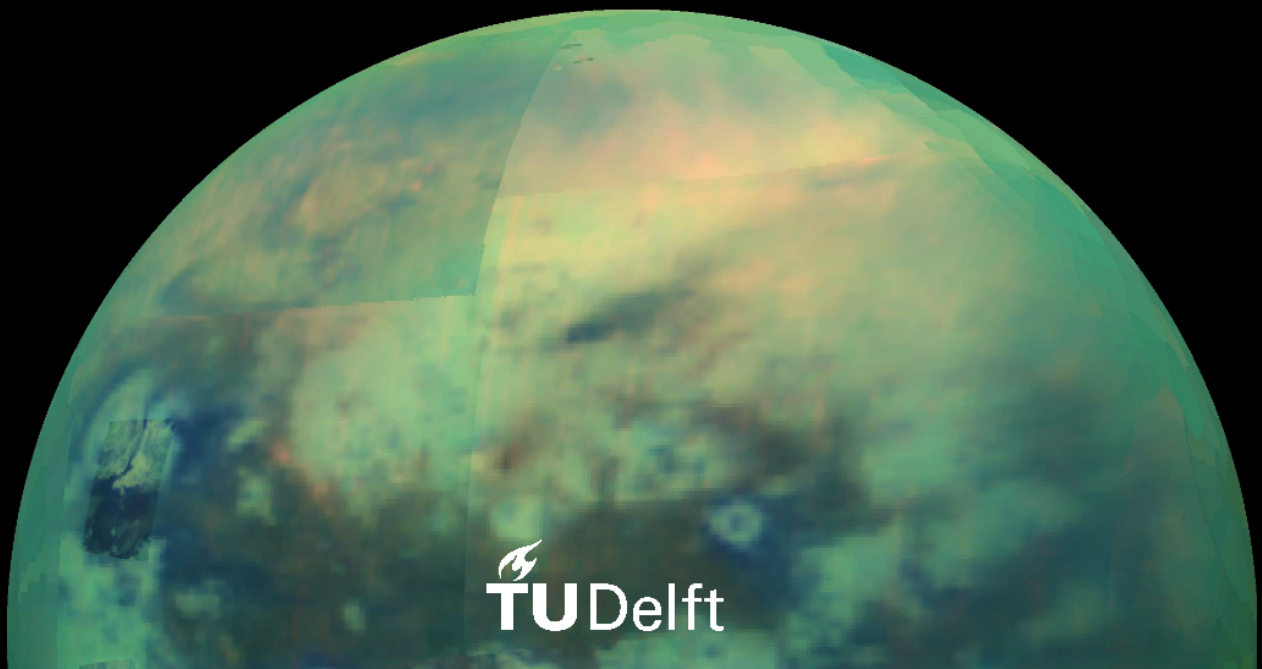

TU Delft

Linking Titan's properties to its formation conditions

A large NH_3 inventory in Titan's building blocks supports the presence of a subsurface ocean

by

C.N. Immerzeel

to obtain the degree of Master of Science
at the Delft University of Technology,
to be defended publicly on Monday July 5th, 2021 at 13:30.

Student number:	4581415	
Project duration:	April 1st, 2020 – July 5th, 2021	
Thesis committee:	Dr. ir. W. van der Wal,	TU Delft, committee chair
	Dr. A. Menicucci,	TU Delft, examiner
	Dr. S. Cazaux,	TU Delft, supervisor
	N. Oberg,	TU Delft, supervisor

Front cover image credits: NASA/JPL/University of Arizona/University of Idaho.
About the object: Composite image of an infrared view of Titan from the Cassini spacecraft.
Back cover image credits: NASA/JPL-Caltech/Space Science Institute
About the object: Natural color view of Titan and Saturn from the Cassini spacecraft.

TU Delft

Preface

This report marks the end of a year of hard work, and could not have been possible without the continued support and encouragement from others. I would like to thank Stéphanie Cazaux, my thesis supervisor. During the DSE you inspired me to pursue space exploration and ever since then you have only helped me learn and grow. You have introduced me to what has become a passion of mine, and there are little things that hold more value than that. Merci beaucoup. I also want to thank Nick Oberg, who has also supervised my work and has provided invaluable contributions. Thank you, for all the discussions and your kind support. A huge thanks to Inga Kamp and Christian Rab, and everyone from the aerospace faculty who has helped me, to Bart Root, Wouter van der Wal, Marc Rovira Navarro, Sean Finck and Alessandra Menicucci.

Grazie Fi, for listening to my many rambles on my thesis, for your words of encouragement and for putting up with me stressing out about circumplanetary disk models at two in the morning. Hopefully I will soon return the favor. I would also like to thank my aunt, Linda, for always taking care of me, and my sibilings, Simón, porque tus consejos ya se echan de menos y Yannita, porque las cosas que me envías siempre me hacen reir. A huge thanks to Misha, for our drunk discussions and forcing me to go on runs that I hate (but not really) way too early in the morning. Gracias Mire, Raquel, Ada, thank you Andrew and thank you to all my beautiful friends, in the Netherlands and in Spain, who brighten up my days and have kept me sane this last year. And last but not least, to the people who have always, and will always, support me; Madre, Padre, siento no llamar más a menudo.

C.N. Immerzeel
Delft, June 2021

Abstract

Gas giant satellites are generally believed to form in circumplanetary disks (CPDs): a gas disk containing solid particles that accumulate to form moons over time. The discoveries by the Cassini-Huygens mission have led to a revision of the birth environment of the Saturnian system.

The aim of this thesis is to constrain the formation circumstances of Titan's building blocks by considering the satellite's observed characteristics, and identify the implications therefrom on Titan's present state. We use the Protoplanetary Disk Modelling (ProDiMo) tool to model radiation thermo-chemical CPDs, and evaluate them on their capacity to reproduce a Titan-like satellite.

To form a moon with Titan's ice-to-rock ratio, we find that the dust-to-gas ratio in the CPD must be in the order of solar nebula values, $log(d/g) = -2.05 \pm 0.2$. The ice availability upon accretion is otherwise incompatible with Titan's moment of inertia. Our models predict a large NH_3 inventory was available upon Titan's formation, ∼10-20wt.% of the total ice. Our findings are consistent with the hypothesis that the observed N_2 in Titan is captured as NH_3, and are compatible with the possible presence of a conductive layer at 45±15 km as revealed by the Huygens probe.

Contents

Nomenclature

Abbreviations and acronyms

A&A	Astronomy and Astrophysics
CEQ	Chemical EQuilibrium
CPD	Circum-Planetary Disk
GCMS	Gas Chromatograph Mass Spectrometer
HASI	Huygens Atmospheric Structure Instrument
MMsN	Minimum Mass sub-Nebula
MoI	Moment of Inertia
MRI	Magneto-Rotational Instability
PPD	Proto-Planetary Disk
ProDiMo	Protoplanetary Disk Model
RDA	Radau-Darwin Approximation
SED	Spectral Energy Distribution
SEMM	Solids Enhanced Minimum Mass
UV	Ultra-Violet

Constants

$\tilde{\rho}_{\mathrm{Titan}}$	Titan mean density	$1.8820 \cdot 10^{3}$ kg m^{-3}
a_{Saturn}	Saturn semi-major axis	$1.4335 \cdot 10^{12}$ m
$L_{\odot}$	Solar luminosity	$382.8 \cdot 10^{24}$ J s^{-1}
M_{Saturn}	Saturn mass	$5.6832 \cdot 10^{26}$ kg
M_{Titan}	Titan mass	$1.3452 \cdot 10^{23}$ kg
$M_{\odot}$	Solar mass	$1.9885 \cdot 10^{30}$ kg
R_{Saturn}	Saturn radius	$5.8232 \cdot 10^{7}$ m
R_{Titan}	Titan radius	$2.5747 \cdot 10^{6}$ m

Elements and molecules

Ar	Argon
C	Carbon
C_2H_2	Acetylene
C_2H_3	Ethylenyl
C_2H_4	Ethylene

C_2H_5 Ethyl radical

C_3H_2 Cyclopropenylidene

CH_3O Methoxide

CH_3OH Methanol

CH_4 Methane

CO Carbon monoxide

CO_2 Carbon dioxide

Fe Iron

FeS Ferrous sulfide

H_2O Water

HCN Hydrogen cyanide

HNO Nitroxyl

N Nitrogen

N_2 (Molecular) Nitrogen

Na Sodium

Ne Neon

NH_3 Ammonia

NO Nitrogen oxide

O Oxygen

OH Hydroxide

PAH Polycyclic aromatic hydrocarbon

Symbols

a_{pow} Powerlaw size index

f_{ice} Ice over total weight

$J_\lambda(r,z)$ Local radiation field

P_{g} Midplane gas pressure

(d/g) Dust-to-gas ratio

α Turbulence

β Flaring index

χ Incident vertical UV

Δv Relative velocity

$\dot{M}$ Accretion rate

ϵ Radial powerlaw index

$\epsilon_{2\mathrm{D}}$ 2D accretion efficiency

ϵ_{3D}	3D accretion efficiency
ϵ_{PA}	Pebble accretion efficiency
η	Headwind prefactor
γ	Tapering-off exponent
Γ_{vis}	Viscous heating rate (per volume)
$\mathcal{P}$	Gap opening parameter
$\mathcal{R}$	Reynolds number
ν	Viscosity
Ω_K	Orbital frequency
ρ	Mass density
ρ_{core}	Core density
ρ_{g}	Gas mass density
ρ_{ice}	Ice density
ρ_{ocean}	Ocean density
Σ	Gas column density
τ_{s}	Dimensionless stopping time
τ_{Titan}	Titan formation timescale
a_{max}	Maximum dust size
a_{min}	Minimum dust size
A_{V}	Optical extinction
c_{s}	Isothermal speed of sound
f_0	Dust size
f_{set}	Modulation factor
F_{vis}	Viscous heating rate (per column)
g	Gravity
$H_{0.1\,\mathrm{au}}$	Reference scale height
H_{g}	Gas scale height
h_{g}	Normalized gas scale height
h_{p}	Normalized pebble scale height
L_{Saturn}	Saturn luminosity
L_{UV}	UV luminosity
M_{CPD}	Disk mass
P	Pressure
p	Scaling parameter

$q_{\mathrm{hw/sh}}$ Transition mass ratio

q_{s} Seed to planet mass ratio

r Radial distance to Saturn

R_{core} Core radius

r_{c} Distance to satellite center

r_{H} Hill radius

$r_{\mathrm{in,CPD}}$ Disk inner radius

$r_{\mathrm{out,CPD}}$ Disk outer radius

r_{s} Seed radius

$r_{\mathrm{taper,CPD}}$ Taper radius

T Temperature

T_{back} Background temperature

T_{d} Dust temperature

T_{eff} Effective temperature

T_{g} Gas temperature

u_{v} Relative flux

v Frequency

v_{*} Transition velocity

v_{hw} Headwind velocity

v_{K} Keplerian speed

v_{sh} Keplerian shear velocity

z Height above the midplane

I Mean MoI

1

Introduction

Titan is similar to Ganymede and Callisto in mass and size, but differs from the Jovian moons in that it is the only large satellite around Saturn, it is host to a massive atmosphere and has a unique internal structure. The parallels between the Jovian and Saturnian systems have led to believe that they both formed in a disk surrounding the giant planets, a cicumplanetary disk (CPD). Hamilton (2013) suggested that the Saturnian system contained initially four massive regular moons, like the Jovian system does, but these collided after an orbital instability event. In this scenario, Titan would have re-acreted from the debris-like disk, and its origin would not be primordial (Hamilton 2013). Differences between the Jovian and Saturnian system architectures have also been explained through distinct mass inflow from the protoplanetary disk (PPD) and the different evolution of a cavity in the disk (Sasaki et al. 2010). Under these different conditions, a single massive satellite can remain in the CPD (Sasaki et al. 2010). Equally, Fujii and Ogihara (2020) show through N-body simulations that a Titan-like satellite can survive inwards migration in the disk for the expected viscosity values. A primordial origin of Titan is therefore possible. The origin of moons inner to Titan, however, remains an issue of debate. Saturn's young rings (Iess et al. 2019), the fast tidal migration of its moons (Lainey et al. 2020), and observations of new moons forming in the rings (Ida 2019), suggest that these moon's formed from the rings, not the CPD (Salmon et al. 2010; Canup 2010; Charnoz et al. 2010; Charnoz et al. 2011; Ćuk et al. 2016). Titan's characteristics constitute thus the most robust constraints on the Saturnian CPD conditions which, in turn, provide clues on the possible uniqueness of satellite system formation mechanisms.

Voyager and Cassini data allowed to constrain Titan's mass, radius and mean density. Titan's gravity harmonics were determined up to degree-three by radio tracking measurements from Cassini (Iess et al. 2010). From these, a moment of inertia (MoI) of 0.327-0.334 (Gao and Stevenson 2013; Tobie et al. 2014), between Ganymede's 0.3105±0.0028 (Anderson et al. 1996) and Callisto's 0.3549±0.0042 (Anderson et al. 2001), could be inferred. Titan's MoI is relevant in that it provides information on the radial mass distribution in the satellite, and is an indicator of the possible chemical composition of the body.

Interior models assume ice fractions ranging from $\sim 30wt.\%$ (Fortes 2012) to $\sim 50wt.\%$ (Grasset et al. 2000; Castillo-Rogez and Lunine 2010). Titan could have three layers: anhydrous rock, a rock/ice mixture and an icy crust (Grasset et al. 2000; Tobie et al. 2005); or two layers: hydrated silicates or an rock/ice mixture surrounded by an icy crust (Fortes et al. 2007; Lunine et al. 2010; Castillo-Rogez and Lunine 2010). A small (<500 km) metallic core cannot be ruled out (Lunine et al. 2010; Fortes 2012). Titan could also host a subsurface ocean (Fortes et al. 2007; Lunine et al. 2010; Fortes 2012), as suggested by Titan's spin state, tidal gravity's response, long-wavelength shape (Tobie et al. 2014) and the measurement of an atypical Schumann-like resonance by the Huygens Atmospheric Structure Instrument (HASI), indicative of the possible presence of a conductive layer at a depth of 45±15 km (Béghin et al. 2010).

The chemistry that is probed via the atmosphere provides further clues to Titan's interior composition and structure. Huygens probe measurements confirmed Titan's atmosphere is primarily composed by N_2 and CH_4 (Gautier and Raulin 1997). Out of the noble gases, only the mole fraction of ^{36}Ar was sampled upon the Huygens probe's descent by the Gas Chromatograph Mass Spectrometer (GCMS), yielding a ratio $(2.06 \pm 0.84) \cdot 10^{-7}$ of ^{36}Ar/(N_2+CH_4) (Niemann et al. 2010). As Ar and N_2 have a

similar volatility and H_2O ice affinity, the Ar/N_2 ratio should be $\sim 5 \cdot 10^5$ times larger than that sampled if the N_2 in Titan was primordial, in order to match the solar composition ratio of $\sim 10^{-1}$ (Niemann et al. 2005; Tobie et al. 2014). Similarly, Titan's atmosphere is depleted in CO with respect to the solar nebula, having $CO:CH_4 \approx 10^{-3}$ (Gautier and Raulin 1997; Mumma and Charnley 2011). With a similar volatility to N_2, the depletion in CO supports the non-primordial origin of N_2. The N_2 in Titan has been suggested to have been captured as NH_3 upon formation (Niemann et al. 2005), a part of which would have outgassed and converted to N_2 by photolysis (Atreya et al. 1978) and shock heating (Jones and Lewis 1987). Titan might thus host a substantial abundance of NH_3 in its interior. Being an anti-freeze, this would support the presence of a subsurface ocean.

The expected primordial species and their abundances in Titan's interior, inferred from observations, should have been present in the satellite's building blocks. For a primordial Titan, the Saturnian CPD conditions should be such that a Titan-like satellite could have formed in it. Despite the fact that astrochemical and interior modelling are related, they are often tackled in isolation. In this thesis, we aim at providing a coherent picture, spanning from Titan's birth environment to the satellite's interior, and assess its implications with regards to satellite formation theory and Titan's characteristics.

1.1. Research questions

Following from the knowledge gaps discussed in the introduction, a research question has been formulated:

What are the predictions of Titan's formation and present state based on its birth environment conditions?

Two questions have been derived from the main research question:

1. What were the characteristics of Titan's birth environment?
   (a) What constraints do the observations of Titan place on its birth environment conditions?
   (b) What CPD characteristics are required to meet the observational constraints?
   (c) What implications do the CPD characteristics have on the environment in which Titan formed?
2. What implications does the chemical composition of the CPD, as a function of radial distance to Saturn, have on the formation of a Titan-like satellite?
   (a) What is the closest distance to Saturn at which Titan could form?
   (b) How does the chemical composition and abundance of the ices in the CPD relate to Titan's present composition?
   (c) What are the predictions that can be made on Titan's radial profile based on the ice and NH_3 availability upon accretion?

1.2. Report outline

The research and findings of this thesis have been documented in the form of a journal article, included in chapter 2. The conclusions and recommendations for future work are provided in chapter 3.

2

Journal article

The research work has been documented in the form of a scientific paper, to be submitted to the journal Astronomy and Astrophysics (A&A). The article is provided in this chapter, following the standard A&A template and guidelines. For consistency in the format, Appendix E: Verification and validation, which will not be submitted for publication, has been included as part of the paper.

Astronomy & Astrophysics manuscript no. output
June 21, 2021

Linking Titan's properties to its formation conditions

A large NH_3 inventory in Titan's building blocks supports the presence of a subsurface ocean

C.N. Immerzeel[1], N. Oberg[1], S. Cazaux[1,2], and I. Kamp[3]

[1] Faculty of Aerospace Engineering, Delft University of Technology, Delft, The Netherlands
[2] University of Leiden, P.O. Box 9513, 2300 RA Leiden, The Netherlands
[3] Kapteyn Astronomical Institute, University of Groningen, P.O. Box 800, NL-9700 AV Groningen, The Netherlands

June 21, 2021

ABSTRACT

Aims. We aim to constrain the environment in which Titan's building blocks formed to assess their relation to the moon's present characteristics.
Methods. We simulate a series of thermo-chemical steady state circumplanetary disks (CPDs). We use interior models to build Titan from the CPD composition (different types of ices) and characteristics (ice-to-rock ratio). We then examine what implications the chemical composition of the CPD has on the formation of a Titan-like satellite.
Results. The dust-to-gas ratio in the CPD must be $(d/g) = 10^{-2.05\pm0.2}$, for Titan to end up with its current ice-to-rock ratio. The ice available upon accretion is otherwise incompatible with the radial mass distribution inferred from Titan's moment of inertia. Our models suggest a large (10-20 wt.%) abundance of NH_3 was available during Titan's formation.
Conclusions. Our findings are consistent with the hypothesis that the observed N_2 in Titan was present in the satellite's building blocks under the from of NH_3, and are compatible with the possible presence of a salty subsurface ocean at a depth of 45±15 km as revealed by the Huygens probe.

Key words. Circumplanetary disk – Titan – Satellite formation

1. Introduction

In the Saturnian satellite system, ~96% of the mass is present in a single moon: Titan. Voyager and Cassini data provided a well constrained $M_{\rm Titan}$ mass, $R_{\rm Titan}$ radius and $\bar{\rho}_{\rm Titan}$ mean density (see Table 1). With radio tracking measurements from Cassini, Titan's gravity harmonics could be measured up to degree-three (Iess et al. 2010). From these, it can be inferred that Titan's mean moment of inertia (MoI) is $I/(M_{\rm Titan}R^2_{\rm Titan}) = 0.3414 \pm 0.0005$, between that of Callisto (0.36) and Ganymede (0.31), assuming hydrostatic equilibrium (Iess et al. 2010). The value extends to 0.334-0.327 when accounting for a possible 5-10% overestimate of the hydrostatic component, respectively (Gao & Stevenson 2013; Tobie et al. 2014).

Table 1: Overview of constants used in this study.

Symbol	Parameter	Value	Unit	Source
$M_{\rm Titan}$	Titan mass	$1.3452 \cdot 10^{23}$	kg	(1)
$R_{\rm Titan}$	Titan radius	$2.5747 \cdot 10^{6}$	m	(2)
$\bar{\rho}_{\rm Titan}$	Titan mean density	$1.8820 \cdot 10^{3}$	kg m^{-3}	(1)
$M_\odot$	Solar mass	$1.9885 \cdot 10^{30}$	kg	(4)
$L_\odot$	Solar luminosity	$382.8 \cdot 10^{24}$	J s^{-1}	(4)
$a_{\rm Saturn}$	Saturn semi-major axis	$1.4335 \cdot 10^{12}$	m	(4)
$M_{\rm Saturn}$	Saturn mass	$5.6832 \cdot 10^{26}$	kg	(1)
$R_{\rm Saturn}$	Saturn radius	$5.8232 \cdot 10^{7}$	m	(3)

References. (1) Jacobson et al. (2006); (2) Zebker et al. (2009) ; (3) Archinal et al. (2018).
[4] Retrieved from https://nssdc.gsfc.nasa.gov/, 21/02/21.

Titan's MoI can be explained by the presence of hydrated silicates in the core [1] and an incomplete rock/ice differentiation. The body could have three layers: anhydrous rock surrounded by a rock/ice mixture and an icy crust. This profile is generally compatible with the lower range of MoI, 0.30-0.33 (Grasset et al. 2000; Tobie et al. 2005). Alternatively, it could have two layers: a rock/ice mix surrounded by ice. A two-layer body could also have a full rock/ice separation, with the possible presence of hydrated silicates (mostly serpentine antigorite) to explain the low core density (Lunine et al. 2010; Fortes et al. 2007; Castillo-Rogez & Lunine 2010).

While no intrinsic magnetic field has been observed, a small metallic core (<500 km) cannot be ruled out, as the core might be barely convecting, or not at all (Lunine et al. 2010; Fortes 2012). Additionally, a subsurface ocean might be present in the outer icy layer, although uncertainties on depth, thickness and composition remain (Lunine et al. 2010; Fortes et al. 2007; Fortes 2012). The existence of a salty ocean is supported by the Huygens Atmospheric Structure Instrument (HASI) measurement of an atypical Schumann-like resonance, which indicates the possible presence of a conductive layer at a depth of 45±15 km (Béghin et al. 2010). An ocean is also suggested by Titan's spin state, tidal gravity's response and long-wavelength shape (Tobie et al. 2014).

While the MoI provides clues to Titan's radial mass distribution, observations of its atmospheric chemistry serve as an

[1] In this paper, core refers to all material inner to an ice crust. For distinct layers within the core, we refer to inner and outer core.

indicator for the interior composition of the satellite. Titan is host to a substantial atmosphere, that consists primarily of N_2 and CH_4, as confirmed by Huygens probe measurements (Gautier & Raulin 1997). Noble gases are present at oversolar abundances both in the atmosphere of telluric planets (Pepin 1992) and that of Jupiter (Owen et al. 1999). In Titan, however, only the mole fraction of ^{36}Ar was clearly sampled upon the Huygens probe's descent by the Gas Chromatograph Mass Spectrometer (GCMS), yielding a ratio $(2.06 \pm 0.84) \cdot 10^{-7}$ of $^{36}Ar/(N_2{+}CH_4)$ (Niemann et al. 2010). Additionally, a tentative $(2.8 \pm 2.1) \cdot 10^{-7}$ of $^{22}Ne/(N_2{+}CH_4)$ was obtained (Niemann et al. 2010). If the large amounts of N_2 that are observed today had been present upon Titan's formation, the Ar/N_2 ratio should be $\sim 5{\cdot}10^5$ times larger (Tobie et al. 2014). Instead, the low amount of ^{36}Ar detected hints towards the capture of nitrogen not as N_2, but as NH_3 (Niemann et al. 2005). Titan's atmosphere has a $CO{:}CH_4$ ratio of $\sim 10^{-3}$ (Gautier & Raulin 1997), while CO is expected to have been more abundant than CH_4 in the protosolar nebula (i.e. Mumma & Charnley 2011). Having a similar volatility to N_2, the depletion in CO suppports the non-primordial origin of N_2. Titan could have accreted NH_3 upon formation and a part of it would have outgassed and converted to N_2 by photolysis (Atreya et al. 1978) and shock heating possibly driven by bombardment (Jones & Lewis 1987). The presence of NH_3, an antifreeze agent, in Titan's interior, would also support the presence of subsurface ocean.

Constraining the birth environment conditions is a key step towards identifying the chemistry of Titan's building blocks and present interior. Gas giant regular satellites are generally believed to form in circumplanetary disks (CPDs): gaseous accretion disks containing dust grains that can be covered in ice. Differences in evolution of a cavity in the disk and mass inflow from the protoplanetary disk (PPD) are often invoked to justify the differences in resulting moon system architectures between the Jovian and Saturnian systems (Sasaki et al. 2010). The birth of the Galilean moons in a CPD has been extensively examined (i.e. Canup & Ward 2002; Mosqueira & Estrada 2003; Sasaki et al. 2010; Miguel & Ida 2016; Cilibrasi et al. 2018; Shibaike et al. 2019; Fujii & Ogihara 2020).

Reconciling the observational constraints with possible formation pathways poses more difficulties when it comes to the Saturnian system. The survival of a single massive satellite as is Titan has often proved challenging. Hamilton (2013) proposed that the Saturnian system contained originally four massive regular satellites, much like the Jovian system does. An orbital instability event would have led to the collision of the moons, resulting on a late debris-like disk from which Titan and mid-sized moons would have formed. A primordial Titan formation is also considered possible: Sasaki et al. (2010) succeeded in simulating the survival of a single massive body in Saturnian-condition systems, and Fujii & Ogihara (2020) demonstrated through N-body simulations that a Titan-mass satellite can remain in the CPD without falling into the planet for a given disk viscosity. Saturn's young rings (Iess et al. 2019), the fast tidal migration of its moons (Lainey et al. 2020), and observations of new moons forming in the rings have, in the last decade, led to a re-evaluation of the origin of Saturn's inner satellites (Ida 2019). Recent studies show that the formation of moons interior to Titan might not have occured within a CPD, but from Saturn's rings (Salmon et al. 2010; Canup 2010; Charnoz et al. 2010, 2011; Ćuk et al. 2016). While these moons might constitute a second generation of satellites, Titan can survive against migration in the CPD (Fujii & Ogihara 2020; Sasaki et al. 2010), and be primordial. Its characteristics constitute thus the most robust constraints on Saturnian CPD conditions.

With the aim of assessing how the chemistry of a primordial CPD can be used to explore Titan's interior structure and composition, we simulate a series of thermo-chemical steady state CPDs. The model inputs are described in section 2, and the resulting CPDs are examined in section 3. In section 4, we identify the required ice-to-rock ratio and the NH_3 ice abundance to form Titan with a MoI comparable to the measurements. We then evaluate the CPDs on their capacity to reproduce said volatile content and identify the range of CPD parameters and distance from Saturn allowing to form Titan with its observed characteristics in section 5. A discussion of the results is provided in section 6, and the conclusions in section 7.

2. Circumplanetary disk models

We use the radiation thermo-chemical disk modelling code ProDiMo (Protoplanetary Disk Model) (Woitke et al. 2009; Kamp et al. 2010; Woitke et al. 2016). The tool self-consistently and iteratively computes the physical, thermal and chemical structure of circumstellar or circumplanetary disks. ProDiMo is fed a set of CPD characteristics. The radiation field at every grid point $J_\lambda(r,z)$ and the local dust temperature $T_d(r,z)$ are computed from a wavelength-dependent continuum radiative transfer. Then, the gas phase and ice chemistry as well as heating and cooling balance can be obtained. Throughout iteration, a model with a consistent density, radiative transfer and chemistry is obtained. The chemical network, consisting of 13 elements and 235 chemical (gas and ice) species, is listed in Table 4 in Kamp et al. (2017). Gas phase and ultra-violet (UV) reactions are obtained from the UMIST2012 database (McElroy et al. 2013).

2.1. Reference CPD model

Table 2: ProDiMo input parameters for the reference Saturnian CPD

Parameter	Symbol	Value	Unit
Saturn mass	$M_{\rm Saturn}$	$2.86 \cdot 10^{-4}$	$M_\odot$
Saturn luminosity	$L_{\rm Saturn}$	10^{-6}	$L_\odot$
Effective temperature	$T_{\rm eff}$	$4.00 \cdot 10^2$	K
UV luminosity	$L_{\rm UV}$	10^{-8}	$L_\odot$
Incident vertical UV	χ	10^2	-
Background temperature	$T_{\rm back}$	30	K
Disk mass	$M_{\rm CPD}$	$3.00 \cdot 10^{-9}$	$M_\odot$
Disk inner radius	$r_{\rm in,CPD}$	10^{-3}	au
Taper radius	$r_{\rm taper,CPD}$	$1.46 \cdot 10^{-1}$	au
Disk outer radius	$r_{\rm out,CPD}$	$4.38 \cdot 10^{-1}$	au
Tapering-off exponent	γ	1.00	-
Radial powerlaw index	ϵ	1.00	-
Flaring index	β	1.15	-
Reference scale height	$H_{0.1\ \rm au}$	10^{-2}	-
Minimum dust size	$a_{\rm min}$	$5.00 \cdot 10^{-2}$	μm
Maximum dust size	$a_{\rm max}$	10	μm
Dust-to-gas ratio	(d/g)	10^{-2}	-
Turbulence	α	10^{-4}	-
Accretion rate	$\dot{M}$	$3.00 \cdot 10^{-11}$	$M_\odot$ yr^{-1}

In this section, a brief description and justification of the main parameter choices for the reference model is provided and

reported in Table 2. An overview of the constants used in this study can be found in Table 1. While radiation dictates the radial temperature structure in PPDs, the temperature in CPDs is dictated by viscous dissipation. The CPD is expected to evolve with time: the disk cools down as accretion declines, and the icelines migrate towards Saturn. Owing to its MoI, Titan is expected to have formed in a minimum of $\sim 10^6$ yrs to prevent melting and differentiation (Iess et al. 2010; Sasaki et al. 2010). For this timescale, the birth environment can be approximated by a stationary disk, without consideration for the iceline migration (Anderson et al. 2021).

The disk model follows a gas mass density distribution (Woitke 2015),

$$\rho_g(r,z) \propto exp\left(\frac{-z^2}{2H_g(r)^2}\right), \tag{1}$$

where r and z refer to radial distance and height above the midplane, respectively. The disk scale height H_g is fully parametrized, and its normalized form follows (Woitke et al. 2011),

$$h_g(r) = \frac{H_g}{r} = H_{0.1\,au}\left(\frac{r}{0.1\,au}\right)^{\beta}, \tag{2}$$

with all simulated disks having reference sale height $H_{0.1\,au} = 0.01$, and a flaring index β=1.15, which are canonical values for a PPD. The gas column density follows from vertically integrating $\rho_g(r,z)$ (Woitke 2015),

$$\Sigma(r) \propto r^{-\epsilon} exp\left(-\left(\frac{r}{r_{taper,CPD}}\right)^{2-\gamma}\right), \tag{3}$$

where $\epsilon = 1.0$ is a radial powerlaw index, $r_{taper,CPD}$ the tapering-off radius and $\gamma = 1.0$ the tapering-off exponent.

Disk dimensions

The model inner radius is approximated by the upper Roche Limit bound, $r_{in,CPD} = 0.001$ au, corresponding to the inner C ring location (Charnoz et al. 2009). While the CPD might have extended further inwards, no moons could form below this limit. The CPD outer radius, $r_{out,CPD}$ is approximated by Saturn's Hill radius as in Canup & Ward (2002),

$$r_H = a_{Saturn}\left(\frac{M_{Saturn}}{3M_\odot}\right)^{1/3}, \tag{4}$$

where r_H is Saturn's Hill radius and a_{Saturn} its semi-major axis, yielding $r_{out,CPD} = r_H = 0.438$ au. The CPD is expected to have been tapered at a distance corresponding to the centrifugal radius of the accreting material, $\sim 0.33 r_H$ (Quillen & Trilling 1998), possibly up to $\sim 0.4 r_H$ according to accretion disk models subject to tidal forces from the central star (Martin & Lubow 2011). We adopt the former, $r_{taper,CPD} = 0.33 r_H = 0.146$ au. This is within 2% of the photoevaporative truncation radius computed from Equation 13 in Oberg et al. (2020) for our input parameters (Table 2).

Disk mass

Based on an actively supplied disk throughout the phase of satellite growth (Canup & Ward 2002), the CPD mass ranges between $10^{-5} - 10^{-4} M_{Saturn}$ (Kronrod & Makalkin 2017). Therefore, with Saturn's mass $M_{Saturn} \approx 3 \cdot 10^{-4} M_\odot$, M_{CPD}=[$3 \cdot 10^{-9} M_\odot, 3 \cdot 10^{-8} M_\odot$]. For the reference model, we adopt the lower bound, $M_{CPD} = 3 \cdot 10^{-9} M_\odot$, as the Saturnian CPD is expected to have formed in a depleted PPD (Sasaki et al. 2010). In section 2.2, we investigate more massive CPDs.

Background radiation field

Unlike relatively isolated PPDs in low-mass star formation regions, the Saturnian CPD could have been exposed to significant UV irradiation from the nearby Sun. To account for this, we consider the CPD to be embedded in an homogeneous vertical radiation field. The FUV can efficiently heat up and affect the chemical composition of the upper molecular layers of a disk. If the CPD has a low dust mass, it can be sufficiently optically thin for the midplane to be irradiated.

In the interstellar medium, $(\nu u_\nu)_{1000\,Å}$ at a wavelength of 1000 Å is $4 \cdot 10^{-14}$ erg cm^{-3} (Habing 1968), with ν the frequency, and u_ν its relative flux. The dimensionless factor χ follows,

$$\chi = \frac{(\nu u_\nu)_{1000\,Å}}{4 \cdot 10^{-14}\ \mathrm{erg\ cm^{-3}}}. \tag{5}$$

Presently, the Sun produces $\approx 10^{-3}$ erg cm^{-2} s^{-1} at 1000 Å[2]. This value is expected to have been significantly higher for the young Sun, namely $\approx$ 100 – 1000 times higher (Ribas et al. 2005). Based on an expected UV radiation field strength at Saturn's location for an unperturbed disk, $\chi \sim 10^2$ (Oberg 2021), we adopt this value for the reference model. Due to the high uncertainty, we examine a wider range of χ in section 2.2.

The background temperature parameter allows to have the CPD embedded in a certain PPD temperature. Saturn is not expected to have opened a gap (Sasaki et al. 2010). Hence, the CPD is considered to be in thermal equilibrium with the surrounding PPD. Makalkin & Dorofeeva (2006) find temperatures in the solar nebula at a distance $r \approx 10$ au are in the range T_{back} = [20, 40] K. We adopt $T_{back} = 30$ K.

Planetary characteristics

The formation of the regular satellites is expected to occur towards the tail end of giant planet accretion, when the planet is approaching its final mass (Charnoz et al. 2009, Sasaki et al. 2010). Because of this, the luminosity considered should coincide with the value after envelope contraction. Having lower mass than Jupiter, Saturn is expected to have had lower initial luminosities (Lissauer et al. 2009, Burrows et al. 1997). An upper bound can be set coinciding with young Jupiter's luminosity, $\sim 10^{-5} L_\odot$ (Lissauer et al. 2009). The lower bound in considered luminosity is obtained from Burrows et al. (1997), $\sim 10^{-7} L_\odot$, corresponding to $T_{eff} \approx 250$ K for a Saturn-mass planet. In the reference model, we adopt $L_{Saturn} = 10^{-6} L_\odot$.

Saturn's effective temperature was considerably higher upon satellite formation: $T_{eff} \approx [250, 500]$ K, corresponding to $L_{Saturn} = [10^{-7}, 10^{-5}] L_\odot$ (Burrows et al. 1997). For the reference model, we adopt $T_{eff} = 400$ K (corresponding to

[2] Retrieved from http://www.sws.bom.gov.au/Educational/2/1/7, 15/02/21.

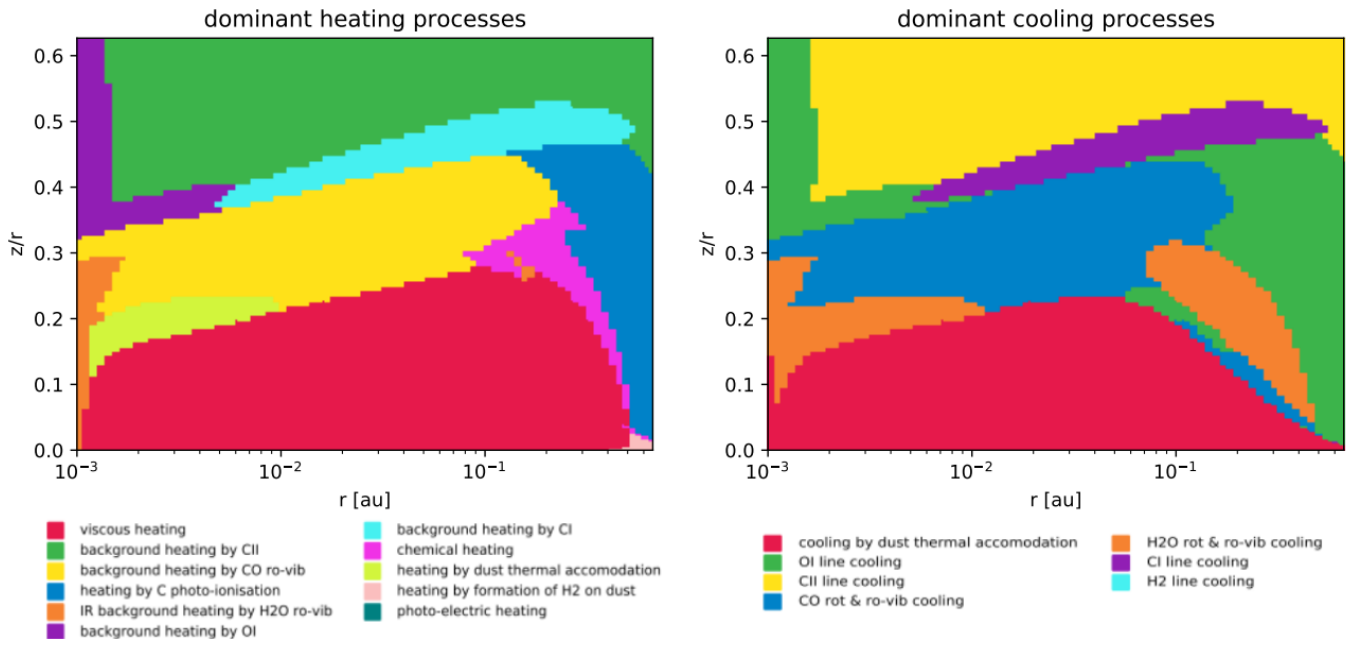

Fig. 1: Dominant heating (left) and cooling (right) processes in the reference CPD. The input parameters are given in Table 2.

$L_{\rm Saturn} \approx 10^{-6} L_\odot$ and $M_{\rm Saturn} = 3 \cdot 10^{-4} M_\odot$ in Burrows et al. (1997)).

Saturn is the principal source of irradiation in the CPD. Its stellar spectrum is approximated by the metallicity atmosphere and evolutionary model ATMO 2020, with Chemical EQuilibrium (CEQ), presented by Phillips et al. (2020) [3]. Our model is provided an input spectrum corresponding to $T_{\rm eff} = 400$ K and $\log(g) = 3.019 \approx 3.0$.

Viscous heating

Unlike PPDs, CPDs are continuously fed by a vertical gas and dust influx (Lubow et al. 1999). These are injected at distances extending to the centifugal radius, where the angular momentum of the inflowing gas equals Saturn's gravitational potential (Canup & Ward 2002). The infalling gas spreads both inwards, onto Saturn, and outwards (Canup & Ward 2002). The former motion implies a reduction of the gas orbital radius r. For the gas to re-adapt to the local Keplerian velocity, a braking force must be in action: an internal, viscous force. Simply put, mass accretion onto Saturn entails an energetic variation: gas kinetic and potential energy decrease and thermal energy increases for an isolated CPD. This increase in thermal energy is referred to as viscous dissipation (Woitke 2015).

To account for the viscous heating rate, models include a mass accretion rate input, $\dot{M}$. This value does not modify the mass of the CPD or include infall (shock) heating. Instead, it is used to compute the viscous dissipation heating on a steady-state disk from a constant inflow. The viscous heating rate is determined from $\dot{M}$ following D'Alessio et al. (1998),

$$F_{\rm vis}(r) = \frac{3 G M_{\rm Saturn} \dot{M}}{8\pi r^3} \cdot \left(1 - \sqrt{R_{\rm Saturn}/r}\right), \quad (6)$$

where $F_{\rm vis}(r)$ is the viscous heating rate per column at a given distance r from the central planet in erg cm^{-2} s^{-1}, and G the gravitational constant.

The models assume (I) a constant $\dot{M}$ across the CPD, (II) that when the disk shrinks, part of the gravitational energy turns to heat and (III) a heating rate vertically distributed as,

$$\Gamma_{\rm vis}(r,z) = \frac{F_{\rm vis}(r) \cdot \rho^p(r,z)}{\int \rho^p(r,z')dz'}, \quad (7)$$

being $\Gamma_{\rm vis}(r,z)$ the energy rate per unit volume locally generated by viscous stress, ρ the mass density and p a scaling parameter, with $p = 2$ in the models (D'Alessio et al. 1998)[4].

To summarize, whether the disk is viscously heated or not, and to which extent, constrains midplane heating and disk chemistry. The viscous heating parameter from Equation 7 is computed from an $\dot{M}$ input through Equation 6. We adopt $\dot{M} = 3.0 \cdot 10^{-11} M_\odot$ yr^{-1}, which is a reasonable value to grow Titan in its expected formation timescale, $\tau_{\rm Titan}$= O(10^6) yr (Sasaki et al. 2010; Iess et al. 2010).

Turbulent viscosity

The effective viscosity of CPDs is still a matter of debate. As given by Shakura & Sunyaev (1973), the standard α definition is,

$$\nu = \alpha c_{\rm s} H_{\rm g} = \alpha \Omega_{\rm K} H_{\rm g}^2, \quad (8)$$

where ν is the viscosity and $c_{\rm s} = H_{\rm g}/\Omega_{\rm K}$ is the isothermal speed of sound (Shakura & Sunyaev 1973); $\Omega_{\rm K}$ refers to the orbital frequency. This allows to define a space and time dependant viscosity, having a constant α CPD and PPD (Estrada et al. 2017). Having no direct observational constraint on CPD viscosity, existing models posit values to fit different scenarios; α is poorly

[3] The theoretical spectra can be retrieved from http://svo2.cab.inta-csic.es/theory/newov2/index.php.

[4] Retrieved from https://forge.roe.ac.uk/trac/ProDiMo/wiki/viscous_heating, 17/02/21

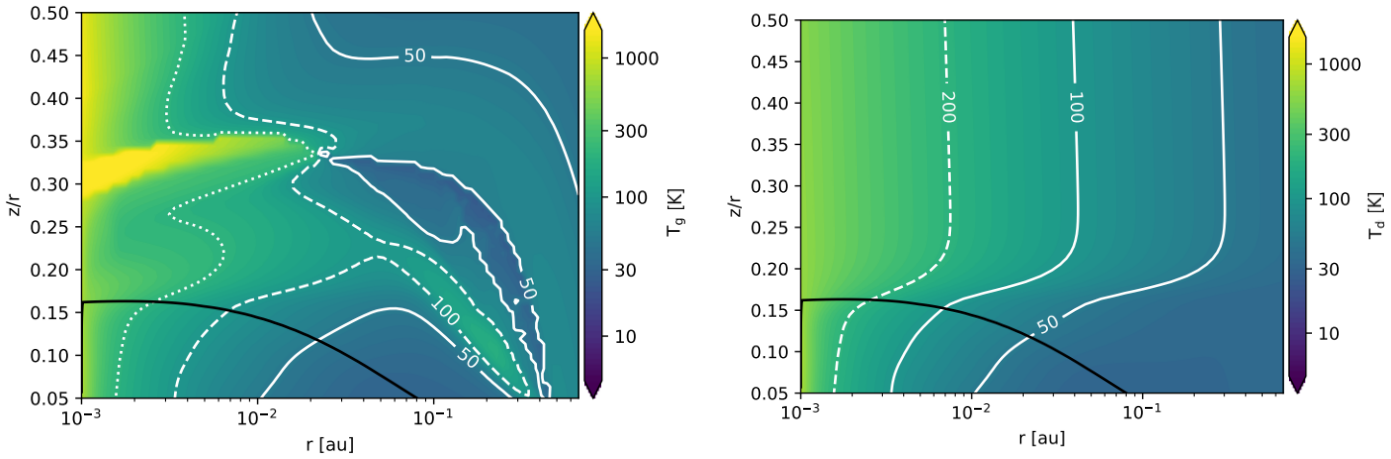

Fig. 2: Gas (left) and dust (right) temperature across the reference model disk. The white contour lines indicate different temperature values, and the black lines mark the location of the optical extinction line, at which A_v=1. The input parameters are given in Table 2.

constrained. Following Ronnet & Johansen (2019) and Shibaike et al. (2019), a turbulent viscosity of $\alpha = 10^{-4}$ is assumed. This value is in agreement with the inability to sustain Magneto-Rotational Instability (MRI) in the CPD, resulting in a low turbulence disk (Fujii et al. 2014). Moreover, Fujii & Ogihara (2020) find $\alpha = 10^{-4}$ to be the most favorable viscosity value for the survival of a single massive moon.

Dust characteristics

Dust grains in the CPD are the main constituent of the accreting satellites, and their properties and abundance constrain moon mineralogy and formation scenarios. Furthermore, they dictate the CPD's opacity and thereby its temperature. Chemical reactions on dust surface and disk turbulence and ionization state are also dependant on the dust (Birnstiel et al. 2012).

At the location of giant planet formation, the dust-to-gas ratio in the solar nebula ranges $(d/g) = (1.49 \pm 0.15) \cdot 10^{-2}$ (Lodders 2003). Based on this, the dust to gas ratio in the reference CPD is approximated by the canonical value $(d/g) = 10^{-2}$. The ratio is varied in section 2.2 to assess its impact on disk characteristics.

Dust abundance and size is assumed to be uniformly distributed across the disk radius (Woitke et al. 2009). For every column, dust size follows a powerlaw distribution before settling, expressed as (i.e. (Woitke et al. 2016)):

$$f_0(a) \propto a^{-a_{\rm pow}}, \tag{9}$$

with $a \in [a_{\rm min}, a_{\rm max}]$, where $a_{\rm pow}$ is the powerlaw size index and $f_0(a)$ is computed to match the imposed (d/g) ratio (Woitke et al. 2009), and $a_{\rm min}, a_{\rm max}$ are the minimum and maximum dust particle size in microns. Dust settling is computed following Dubrulle et al. (1995), finding an equilibrium between settling caused by gravity and diffusion caused by turbulence. In this context, the dust scale height decreases with distance to the planet, while gas scale height becomes increasingly flared (Woitke 2015). While small particles are the main contributors to dust surface area and opacity, large particles are the main contributors to dust mass (Woitke et al. 2016).

Draine (2006) finds a PPD grain distribution that can account for the observed submillimiter opacity of interstellar dust, characterized by $a_{\rm pow} \approx 3.5$ and $a_{\rm max} \geq 3$ mm. Since Saturn is not expected to have formed a gap (Sasaki et al. 2010), incoming grains from the PPD may not be filtered by pressure-bumps. However, we investigate a CPD corresponding to the tail end of planet formation. Due to the fragmentation and drift of dust, maximum particle size becomes smaller in time. Therefore, we adopt $a_{\rm pow} = 3.5$ and $a_{\rm max} = 10\mu$m. In the Inter-Stellar Medium (ISM), observed wavelength dependence of extinction is matched by a 3.5 power-law index with $a_{\rm min} = 0.05\ \mu$m (Mathis et al. 1977), which we take as the minimum particle size in the CPD. For the opacity calculations, we assume the dust grains are 60% amorphous silicate, $Mg_{0.7}Fe_{0.3}SiO_3$, 15% amorphous carbon and porous, with 25% vacuum (Woitke et al. 2016).

2.2. Variation of parameters

Table 3: Varied input parameters for the steady-state CPDs with equilibrium chemistry in ProDiMo

Parameter	Symbol	Reference model	Variations	Unit
Saturn luminosity	$L_{\rm Saturn}$	10^{-6}	10^{-7}, 10^{-5}	$L_\odot$
Incident vertical UV	χ	10^2	10^0, 10^4	-
Disk mass	$M_{\rm CPD}$	$3.00 \cdot 10^{-9}$	10^{-8}, 10^{-6}	$M_\odot$
Dust-to-gas ratio	(d/g)	10^{-2}	10^{-3}, 10^{-1}	-

As described under section 2.1, several of the properties of the Saturnian CPD at the time of Titan's formation are poorly constrained. We find that variation of $\dot{M}$ in a range $\dot{M} = [10^{-11}, 10^{-14}] M_\odot\ {\rm yr}^{-1}$ and variations within $T_{\rm back} = [20, 40]$ K have a negligible impact on the dominant chemical abundances (see Appendix A). We thus focus our attention on the influence that the parameters in Table 3 have on the thermo-chemical disk properties. We run models with the inputs of Table 2, applying the modifications described in Table 3.

3. Results: CPD characteristics

Under the conditions summarized in Table 2, we model the reference disk and obtain the dominant heating and cooling mechanisms shown in Figure 1. Viscous heating, derived from the flow of mass across the CPD, is found to be the dominant heating process. Dust thermal accommodation, where inelastic collisions between dust and gas are coupling their temperature in the optically thick regime, is a dominant coolant. These are of partic-

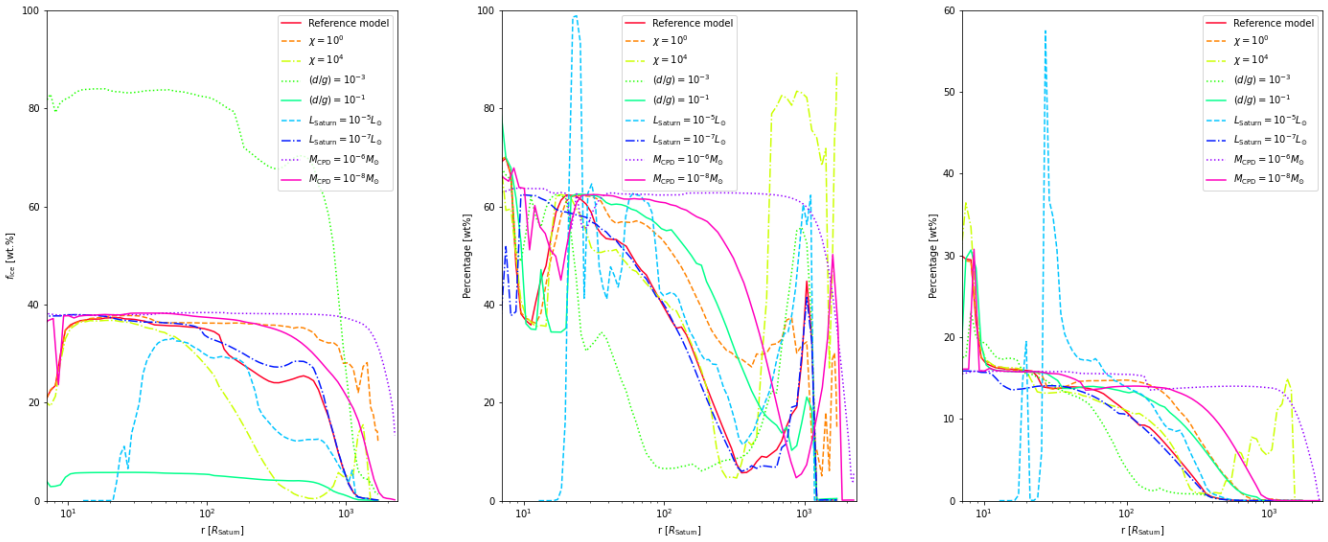

(a) Ice over total weight. (b) H_2O+OH ice over total ice weight. (c) NH_3 ice over total ice weight.

Fig. 3: Column integrated weight percentage as a function of distance to Saturn for the reference model and varied parameters.

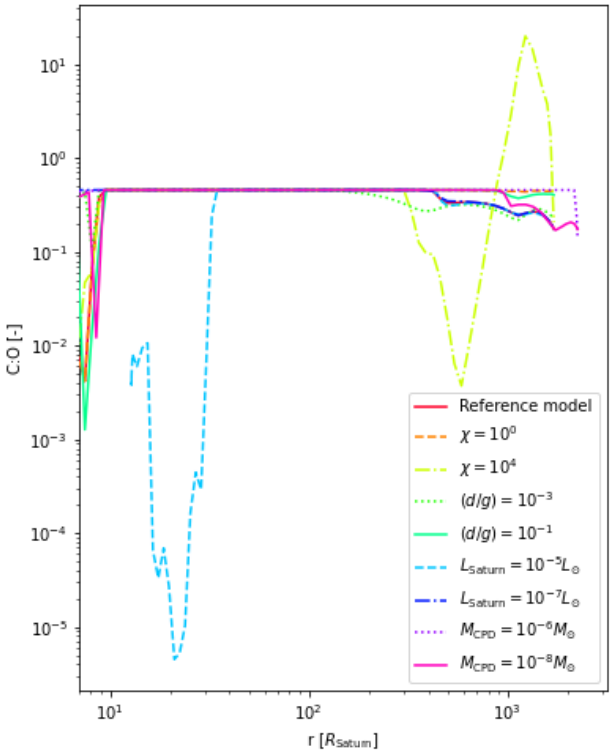

Fig. 4: C:O ratio in the ices for the reference model and varied parameters, as a function of r. The input parameters for the different models are described in section 2.

ular interest as they determine the midplane conditions, where Titan forms. From heating and cooling processes, the thermal balance can be determined and gas and dust temperatures can be derived. The 2D gas and dust temperature structure is shown in Figure 2. We evaluate the model on H_2O ice and NH_3 ice abundance (hereafter referred to as H_2O and NH_3). The icelines are found at 153.5 K and $r = 4.96 R_{\rm Saturn}$ for H_2O and at 96.5 K and $r = 8.82 R_{\rm Saturn}$ for NH_3.

In addition to the reference model, we consider the parameter explorations described in section 2.2. The gas and dust temperatures for all models is shown in Figure A.3, while the most abundant chemical ice species present are depicted in Figure A.4. The column integrated values for the ice over total mass percentage $f_{\rm ice}$, and the H_2O+OH and NH_3 ice over total volatile mass percentages are depicted in Figure 3.

The total ice content $f_{\rm ice}$ as a function of radius is shown for the different models in Figure 3a. The ice content varies by $< 10 wt.\%$ from 10-100 $R_{\rm Saturn}$. The sole exception being the $L_{\rm Saturn} = 10^{-5} L_\odot$ model. There, the disk has a larger $r_{\rm CPD,in}$ as the modelled Saturn has a larger radius, and the H_2O and NH_3 icelines are located at $r \sim 21 R_{\rm Saturn}$ and $r \sim 33 R_{\rm Saturn}$, respectively. We find that the dust-to-gas ratio is the parameter most affecting the ice abundance in Figure 3a, by up to $\sim 45 wt.\%$ at a given r for a change of one in order of magnitude. For the same disk mass, an enhancement of solids implies an increase in surface area, which in increases the optical extinction $A_{\rm V}$, resulting in a disk depleted in volatiles, as is the case when $(d/g) = 10^{-1}$.

Figure 3b shows the percentage of H_2O and OH ices relative to the total ice content as function of radius from Saturn. Both species are considered since OH + H $\rightarrow$ H_2O is a radical-radical reaction that will take place once reactants encounter each other on the surface. Owing to the low desorption energy of OH (i.e. Cuppen & Herbst 2007), this is expected to be in the form of H_2O in Titan's interior. Water content, H_2O and OH, drops for $r > 80 R_{\rm Saturn}$ to $< 50 wt.\%$ ice. In Figure 3c, the NH_3 is presented as a function of radius for the different considered models. The NH_3 content is similar for all models in the 10-100 $R_{\rm Saturn}$ range, and varies by less than 10%. The sole exception is $L_{\rm Saturn} = 10^{-5} L_\odot$ and $(d/g) = 10^{-3}$. The peak in NH_3 at $\sim 12 R_{\rm Saturn}$ in the former corresponds to an outlying low H_2O content.

The C:O ratio, shown in Figure 4, remains constant for all models, with a value ~ 0.46. With the initial elemental ratio be-

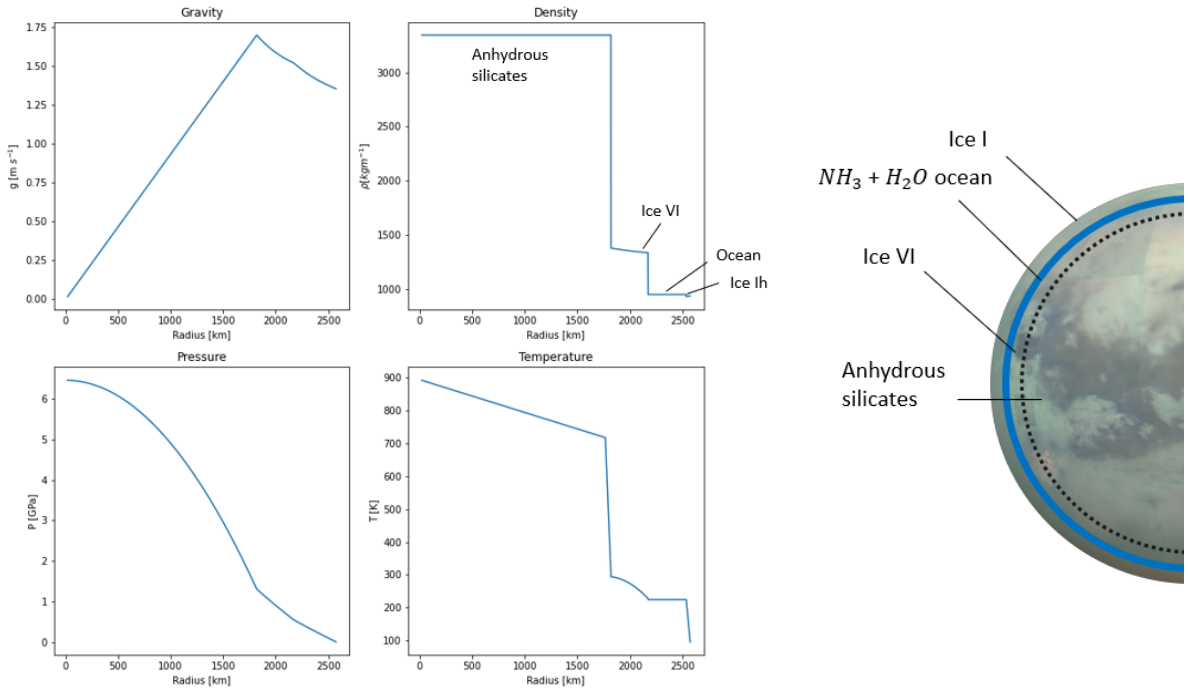

Fig. 5: Characteristics of an anhydrous silicate core and an ammonia rich ocean Titan profile, for in-situ formation at its present location in the reference model. The corresponding conditions are marked with a red star in the top left graph in Figure 6. On the left, profiles of gravity, density, pressure and temperature inside Titan are given. On the right, a depiction of the modelled layers is provided (not to scale). Numerical results for this interior model are provided in Table B.1. Titan image credit: NASA/JPL/University of Arizona/University of Idaho.

ing C:O=0.457 for all CPDs, this indicates all available C and O is being frozen. The decrease in H_2O+OH in Figure 3b corresponds mainly to an increase in CO_2 abundance in our CPDs. The $(d/g) = 10^{-3}$ model is the one containing the highest CO_2 ice content, ~50% of the total ice at $\sim 100 R_{\rm Saturn}$ (as indicated by a bright green line in Figure A.4), and lowest NH_3 content, <10wt.% after $\sim 70 R_{\rm Saturn}$. After CO_2, the most abudant carbon-bearing species in our models are C_2H_2, C_2H_3, C_2H_4, CH_3O, and C_3H_2.

Interior models predict CO_2 to be the main carbon-bearing species in the Saturnian CPD (Tobie et al. 2012; Alibert & Mousis 2007). Waite et al. (2017) find from Cassini measurements of the plumes of Enceladus that CO_2 is present with a 0.3-0.8% volume mixing ratio. This supports the presence of CO_2 in Titan's building blocks, which has been suggested to be the source of Titan's CH_4 as serpentinization by fluids containing CO_2 can produce CH_4 (Zolotov et al. 2005). However, there has been no detection of CO_2 on Titan's surface (Solomonidou et al. 2020; Hartung et al. 2006), and the CO_2 abundance in the CPD remains unknown. Consequently, we do not use CO_2 as a constraint when evaluating the CPDs in their capability to form Titan.

4. Forming Titan

Assuming Titan forms with the same $f_{\rm ice}$ and NH_3 percentages that are present in the disk, we consider a suite of interior models to assess which building blocks yield Titan's MoI, mean density and radius.

4.1. Titan's MoI

A satellites' MoI is related to its radial mass structure following,

$$\frac{I}{MR^2} = \frac{8}{3}\frac{\pi}{MR^2}\int_0^R \rho(r_{\rm c}) r_{\rm c}^4 dr_{\rm c}, \tag{10}$$

where r_c is the distance from the center of the satellite. With radio tracking measurements from Cassini, Titan's gravity harmonics could be measured up to degree-three, with high confidence up to a degree-two (Iess et al. 2010). The precession rate provides the final constraint to compute the principal MoI. Being unavailable for Titan, the Radau-Darwin Approximation (RDA) is applied. The RDA assumes a fluid response to rotational and tidal forces (Fortes 2012). With the RDA, it can be inferred that Titan's normalized MoI is $I/(M_{\rm Titan}R^2_{\rm Titan}) = 0.3414 \pm 0.0005$ (Iess et al. 2010). In order to compute the moment of inertia of Titan with the RDA, an homogeneous interior in hydrostatic equilibrium is assumed (Tobie et al. 2014; Gao & Stevenson 2013). However, gravity and topography measurements indicate that Titan is not in hydrostatic equilibrium but has lateral variations in mass distribution (Gao & Stevenson 2013). These contribute to the observed gravity field, which does not solely reflect a radial mass distribution (Tobie et al. 2014). Consequently, the MoI value that is computed assuming hydrostatic equilibrium requires a correction; an overestimate of the hydrostatic parts between 5 – 10% implies a MoI of 0.334-0.327, respectively (Tobie et al. 2014).

In this work, we refer to a MoI ranging between 0.33 and 0.34 to account for the uncertainties from the different models and for the fact that the value should be lower than the one resulting from the RDA approximation.

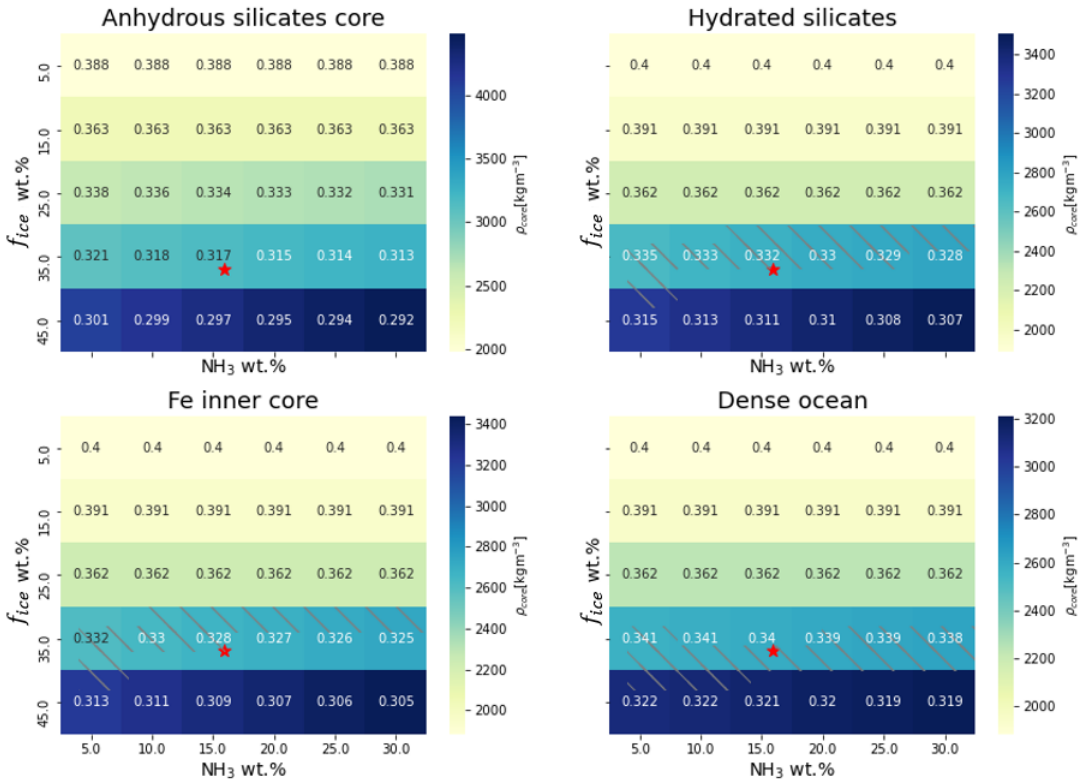

Fig. 6: MoI values as a function of $f_{\rm ice}$ and NH_3 over ice weight percentage. The cell color indicates the core density as described on the color bar right to every sub-figure. The red star indicates the conditions at Titan's current location (r≈ $21R_{\rm Saturn}$) in the reference CPD model. The hatched area indicates which models are in agreement with the constraints described in text.

4.2. Interior models

We have extracted radial profiles of ice and ammonia abundance from our CPD model ensemble (as shown in Figure 3). We assume all ice other than NH_3 ice to be H_2O, which is generally true up to ~ $100R_{\rm Saturn}$, as the liquidus curves for the NH_3-H_2O system are well known (i.e Sotin et al. 1998) and observations do not place constraints on the carbon-bearing species in Titan's interior (see section 3). The presence of other ices in our CPDs is further discussed under section 6. The moon interior models are constrained by Titan's observed density and radius, and an input $f_{\rm ice}$ and NH_3 content. We leave the core density and core radius as unconstrained parameters.

We consider whether conditions within the CPD allow for the in-situ formation of Titan. In reality, Titan is expected to have migrated inwards (i.e. Canup & Ward 2002, 2006) and possibly outwards (Fujii & Ogihara 2020) through tidal interaction with the CPD gas. The implications of migration for Titan's final bulk composition are discussed in Appendix C. The volatile inventory might vary upon encountering a change in conditions due to radial drift. Considering the cold CPD conditions, radial drift is not expected to have had a significant impact on the ice and NH_3 inventory, which are close to constant within 10-100 $R_{\rm Saturn}$ for the reference model (see section 3). The migration of solids in the disk is not expected to have a significant effect on our volatile inventory.

To model Titan's interior, we start by defining the icy layer structure: we first consider the possible presence of an ocean following the method described in Grasset et al. (2000), with which we constrain the ice I layer thickness such that the global heat flux through the ice I shell is equal to the global heat flux from the core. Models having ≥ 3wt.%NH_3 can have an ice I shell matching the heat flux from the core. These models present an NH_3-rich ocean between an ice I layer and high-pressure ices (V-VI). The thickness of the Ice I shell is such that thermal equilibrium is reached. The temperature at the layer bottom follows from the NH_3-H_2O liquidus curve. We assume that the ocean is isothermal, and calculate its depth from the liquid to high-pressure ice transition. The extent of the high-pressure ices is determined by the input $f_{\rm ice}$ parameter. The pressure profile is computed assuming hydrostatic equilibrium. Having the pressure and temperature conditions of the icy layer, we obtain the H_2O ice densities and phases using the open source SeaFreeze software hosted on GitHub[5]. The ammonia rich ocean density is taken from Hammond et al. (2018),

$$\rho_{\rm ocean} = 1.0 + a(T - 273.1) + b(T - 273.1)^2 \quad {\rm g\,cm^{-3}}, \qquad (11)$$

where $a = 1.7{\cdot}10^{-3}$ and $b = 1.3{\cdot}10^{-5}$. We iterate to obtain a self-consistent pressure, temperature and density profile. One of these models is shown in Figure 5, for which an NH_3 content of ~16wt.% yields an ocean extending ~370 km, underlain by ice VI.

Models in which NH_3 is ≤3wt.% result in a fully frozen body, as no layer outer to an ocean can have a heat flux matching that of the core. In this case, we impose temperature profiles from thermal models, following Grasset et al. (2000), and build a fully frozen profile in hydrostatic equilibrium (see 9.2.1.1. in Fortes 2004).

[5] Retrieved from https://github.com/Bjournaux/SeaFreeze, last visited 06/05/2021.

Independently of the NH_3 content, models containing less than 15% ice by weight cannot yield both Titan's mean density and a MoI of 0.33-0.34. The MoI exceeds the observed range as a large portion of Titan's mass is placed close to the surface. In these cases, we approximate the icy layer density by a constant $\rho_{\rm ice} = 1000$ kg m^{-3}.

With the icy layer structure being defined by the ice and NH_3 percentages, we study three core profiles, and a dense ocean profile. Figure 6 shows the MoI values that result for a range of $f_{\rm ice}$ and NH_3 percentage, for each of these four interior profiles. First, we consider a fully differentiated anhydrous core, top left in Figure 6 (profile characteristics are provided in Figure 5). For the second profile, we look at possible ice contents in the core and use antigorite as a reference, which has up to ∼13wt% of H_2O (Ulmer & Trommsdorff 1995). We place this ice percentage in the core, to account for either the presence of hydrated silicates or partial differentiation (Figure B.1). The MoI values for this profile are shown at the top right in Figure 6. The presence of a Fe (or FeS) core cannot be ruled out (Lunine et al. 2010; Fortes 2012). On that account, we include a third model containing a pure Fe core making up 2% of Titan's mass, surrounded by hydrated silicates. The resulting moon characteristics can be found in the bottom left graph in Figure 6, and the corresponding interior profile is shown in Figure B.2.

Deschamps et al. (2010) suggest CH_3OH could be if not the main, an anti-freeze agent in Titan's ocean. In our CPD models, CH_3OH does not stay above 5% for a range larger than $2R_{\rm Saturn}$ in any model. However, CH_3O, which is likely to become CH_3OH during accretion, reaches up to $\sim 36wt.\%$ at $r < 11R_{\rm Saturn}$ in our reference model (see Figure A.4). A content of 5 wt.% CH_3OH has an anti-freeze effect equivalent to that of 3 wt.% NH_3 (Deschamps et al. 2010), and its presence in our CPDs indicates it could exist in Titan's ocean. However, as it is abundant over a very narrow radial range, $r < 11R_{\rm Saturn}$, we neglect its effect on the satellite's mass distribution. That being said, the NH_3 aqueous solution might contain other solutes, such as magnesium sulfates or sodium sulfates, resulting in an ocean density increase. These are not included in the CPD chemical network; we account for their possible presence by considering a dense ocean model ($\rho_{\rm ocean} = 1200$ kg m^{-3} after Fortes (2012)) bottom right in Figure 6, and observe the increase of the MoI.

The different scenarios considered in this study result in different MoIs, which can be seen in Figure 6. We evaluate the CPDs on the capability to form a Titan with both MoI between 0.33-0.34 and an (outer) core density above 2500 kg m^{-3} in the hydrated silicates case and 3000 kg m^{-3} in the anhydrous silicates case. The density constraints ensure, for example, that the anhydrous silicates case does not have a core with densities corresponding to hydrated silicates ($\rho <$ 3000 kg m^{-3}). That is, that the core density results are self-consistent with the assessed scenario. The dashed area in Figure 6 marks the combination of $f_{\rm ice}$ and NH_3 percentages that produce models compatible with the constraints. It can be seen how the anhydrous silicates model (top left in Figure 6) cannot yield a MoI of 0.33-0.34 and have anhydrous core densities.

As we are considering an average core density, the MoI is overestimated in Figure 6. In reality, the density should be higher towards the center and less at outer radii. Under a constant density assumption, the MoI remains accurate up to the third decimal point (see section D.2). Therefore, the present approximation is sufficient to discard a combination of interior structures.

5. Results: Forming Titan

In section 4, we have considered a range of interior profiles for Titan to identify what $f_{\rm ice}$ and NH_3 percentage is consistent with $\bar{\rho}_{\rm Titan}$, $R_{\rm Titan}$ and the MoI. We assess the CPDs obtained in section 3 on their capacity to reproduce the required $f_{\rm ice}$ and NH_3 percentage, as a function of radial distance to Saturn.

5.1. Interior profile

It follows from Figure 6 that, in order to form a Titan with a MoI of 0.33-0.34, the core cannot be fully differentiated and anhydrous. The interior profiles matching the MoI, mean density and radius of Titan require ice to be present in the core and a total ice content of 30-40wt.%. If the ocean density is increased to $\rho_{\rm ocean} = 1200$ kg m^{-3} to account for the possible presence of salts, the total ice content must be between 35-40wt.% to be in agreement with MoI observations. A satellite with a MoI of 0.33-0.34 and an ice fraction of 30-40% can only form when our adopted $(d/g) = 10^{-2}$, implying that the dust-to-gas ratio in our models must be on the order of solar nebula values upon Titan's formation. For the other dust-to-gas ratios considered in Table 3, $f_{\rm ice}$ does not change enough to match a MoI of 0.33-0.34 even for the range of χ, $L_{\rm Saturn}$ and $M_{\rm CPD}$ values we consider (see Figure 3).

In the absence of anti-freeze impurities, Titan might be fully frozen (Grasset et al. 2000). Ammonia (NH_3), and potentially other anti-freeze species, allow for the presence of a subsurface ocean. The latter replaces higher density ice phases II and V, thus reducing the MoI. Although the MoI is more strongly dependent on the bulk ice fraction of the satellite, a higher abundance of NH_3 produces a deeper ocean and a relatively smaller MoI. An icy layer enriched in 5, 10 and 15wt.% NH_3 results in ocean depths of 274, 324 and 359 km at distance from the surface of 80, 53 and 39 km, respectively. For a hydrated core model with 35wt.% ice, the corresponding MoI are 0.335, 0.333 and 0.332. To reproduce a MoI of 0.33-0.34, the body cannot contain more than 21wt.% NH_3 in the ice layer, regardless of $f_{\rm ice}$, as in indicated in Figure 6. Said amount can be up to 33wt.% for a model ocean enriched with other solutes, like magnesium sulfates or sodium sulfates. As described in section 3, our models suggest that a large NH_3 reservoir was available at Titan's formation: in the reference CPD model, NH_3 content is more than 15wt.% within $28R_{\rm Saturn}$, and more than 10wt.% NH_3 up to r≈$111R_{\rm Saturn}$. These high values result in thick oceans, decreasing the relative mass fraction of the outer layers.

5.2. Where Titan forms

In Figure 7, we show the MoI of a satellite formed in our reference CPD model. Our CPD model provides the $f_{\rm ice}$ and NH_3 content at each radial location within the disk. In this CPD model, Titan must have obtained the bulk of its mass between ∼11-$130R_{\rm Saturn}$, due to the lack of ices outside these boundaries. At $80 - 130R_{\rm Saturn}$, Titan forms with $< 50wt.\%$ H_2O+OH in the ices, while carbon-bearing species become abundant (see discussion under section 3).

Titan's orbital expansion rate has been found to be 11.3±2.0 cm yr^{-1}, significantly faster than previously assumed (Lainey et al. 2020). This results in a substantial outwards migration over Titan's lifetime, which suggests that the moon was in close proximity to the planet upon disk dispersal, $\sim 5R_{\rm Saturn}$ according to Equation 17 in Supplementary Information in Lainey et al. (2020). The accretion efficiency of Titan increases with Ti-

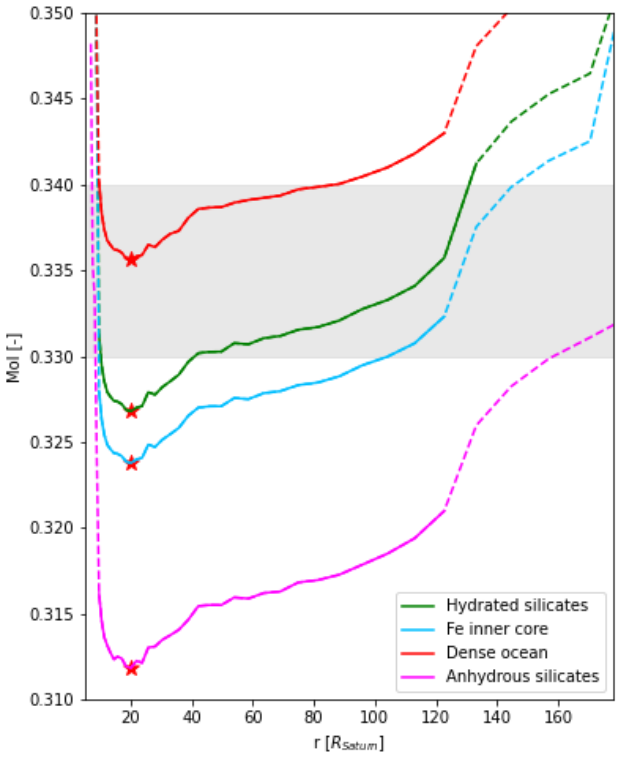

Fig. 7: MoI of model Titan if formed in-situ at every radial distance from Saturn, for reference model characteristics and interior profiles described in section 4.2. The dashes lines indicate core densities not meeting the constraints described in text, while the shaded area marks the observed MoI. The red stars correspond to those in Figure 6, and mark Titan's present location in the disk.

tan's seed mass and in proximity to Saturn (see Appendix C). Consequently, Titan is expected to have accreted more than half of its mass in less than $\sim 10 R_{Saturn}$ of its final migration location (Appendix C). If Titan stopped growing at $\sim 5 R_{Saturn}$, the bulk of its mass should have been acquired closer than $\sim 15 R_{Saturn}$ from the planet. We assess our CPDs to determine whether Titan could have formed in proximity to Saturn from a thermochemical standpoint.

CPD models allowing for the closest formation of Titan are $M_{CPD} = 10^{-6} M_{\odot}$ and $L_{Saturn} = 10^{-7} L_{\odot}$. The former value is in line with a Minimum Mass sub-Nebula (MMsN) model (Lunine & Stevenson 1982), and reduces the minimum distance to the planet to $\sim 4\ R_{Saturn}$ by increasing the optical extinction A_V, allowing ices to form and survive. The forming moon must, however, contain a significant ice fraction in its core to match the MoI, which contradicts the fast formation timescales that take place in such a massive CPD, even at larger distances. Consequently, the only birth environment that is compatible with Titan acquiring the bulk of its mass closer than 7 R_{Saturn} requires $L_{Saturn} = 10^{-7} L_{\odot}$. This luminosity can be reached $\sim 10^{7.3}$ yrs after Saturn's formation (Burrows et al. 1997), while Saturn's CPD is expected to have a lifetime of $\sim 10^6$-10^7 yrs (Alibert et al. 2005; Castillo-Rogez et al. 2009; Shu et al. 1993). Titan formed in the latest stages of the CPD (Charnoz et al. 2009; Sasaki et al. 2010), and could have experienced $L_{Saturn} = 10^{-7} L_{\odot}$ upon accretion. For $L_{Saturn} = 10^{-7} L_{\odot}$ in our models, it is possible that Titan stopped growing at $\sim 5 R_{Saturn}$.

Conversely, increasing the luminosity to $L_{Saturn} = 10^{-5} L_{\odot}$ moves the H_2O iceline outwards to $r \approx 21 R_{Saturn}$ (see section 3). Under such conditions, there is not enough ice to form a satellite matching Titan's observed characteristics at distances closer than $\sim 42 R_{Saturn}$ (see Figure 3a). While this is the only model inhibiting formation of Titan closer than $\sim 15 R_{Saturn}$ from the planet, the luminosity of Saturn is expected to have dropped below $L_{Saturn} = 10^{-5} L_{\odot}$ after only 10^5 yrs (Pollack et al. 1977). This parameter choice, which hinders the formation of Titan in close proximity to the planet, reflects conditions are not expected to have been experienced by the growing satellite. Other than $L_{Saturn} = 10^{-5} L_{\odot}$, all our CPDs are compatible with the the formation of Titan as close as $\sim 7 R_{Saturn}$. The $\sim 5\ R_{Saturn}$ distance suggested by (Lainey et al. 2020) is only possible for a low Saturn luminosity, $L_{Saturn} = 10^{-4} L_{\odot}$, which reduces the minimum radial distance for formation to $\sim 4 R_{Saturn}$, and can take place if Titan formed in the latest stages of the CPD, which is expected (i.e. Charnoz et al. 2009; Sasaki et al. 2010).

While our CPDs, excepting $L_{Saturn} = 10^{-5} L_{\odot}$, allow for the formation of Titan in proximity to Saturn, they do not place a clear upper limit on the radial distance at which Titan can form. We consider an external UV radiation field strength $\chi = 10^4$ reflecting a time at which the young Sun had an excess UV component. This strong UV mostly affects the outer regions of the CPD, and still allows for enough f_{ice} and NH_3 ice to be present to form Titan, albeit over a smaller radius ($r \lessapprox 81 R_{Saturn}$). By contrast, a very low solar radiation of $\chi = 10^0$ extends it to a maximum $r \approx 218 R_{Saturn}$. While the reduced accretion efficiencies at such far distances from the planet do not support this scenario (see Figure C.1), placing stringent upper limits on Titan's r upon formation requires a more in-depth study of the accretion and migration process.

6. Discussion

We have assumed that f_{ice} in the CPD directly translates to how much ice there is presently in Titan's interior. In reality, a fraction of the volatiles available in the CPD could be lost either during or after their accretion onto Titan.

The accretion process could be imperfect, meaning only part of an impacting body is accreted onto the growing satellite. In this scenario, part of the ice can be lost from Titan by vaporization and subsequent escape. Dwyer et al. (2013) finds an Europa-like body's ice fraction can decrease from 0.53 to 0.48 by this mechanism, and up to 0.44 if the vapor escape threshold (impact to escape velocity) is relaxed from 5 to 2. Considering the upper bound, up to 9% of the initial ice mass could be lost from Titan due to imperfect accretion. Water molecules can also be lost through the atmosphere through hydrodynamic escape. For Titan's accretion timescale, $\sim 10^6$ yrs (Iess et al. 2010; Sasaki et al. 2010), warming from the background disk is more important than the mass accreted in determining the reach of hydrodynamic escape (Bierson & Nimmo 2020). For our reference model, background temperatures are lower than ~ 100 K in the midplane for $r > 8 R_{Saturn}$ (see Figure A.3). For this temperature and formation timescale, hydrodynamic escape has a negligible effect on the body's density (see Fig. 3 in Bierson & Nimmo 2020).

Another process that could lead to the loss of Titan ices is the stripping of volatiles through giant impacts. The inner cav-

ity could be absent in the Saturnian CPD, leaving satellites to migrate freely towards Saturn (Sasaki et al. 2010). As the satellites do not pile up in a resonance chain, collisions between larger bodies are likely to have taken place in the Saturnian CPD (Dwyer et al. 2013). Titan may have offered an environment favorable for bombardment, which has been proposed to be at the origin of the conversion of NH_3 to N_2 via shock heating (Jones & Lewis 1987). According to Nimmo & Korycansky (2012), an impactor of ~5 times the mass of Enceladus colliding at 10 km s^{-1} would only vaporize ~0.04 of the mass of Titan. Such an energetic impact would yield a fully differentiated Titan (Brian Tonks & Jay Melosh 1992; Estrada & Mosqueira 2006), not reconcilable with thermal evolution constraints from Titan's MoI (see section 4 for detailed discussion). We take this value, ~0.04 of Titan's mass, as a generous upper bound for how much ice could be lost due to giant impacts. Ice could also be lost due to tidal heating. In order to determine the upper bound in mass that could be lost due to this mechanism, we consider eq. 5 in Dwyer et al. (2013). Even if Titan sustained its highest tidal-heating flux (1.9 TW, Grasset et al. (2000)) for a very extended period ($3 \cdot 10^9$ yrs) with none of the lost volatiles being reaccreted, Titan's loss in $f_{\rm ice}$ would decrease in less than 1% with respect to $f_{\rm ice}$ in the CPD.

Imperfect accretion, hydrodynamic escape, high-velocity impacts and tidal heating can lead to a decrease in ice in Titan with respect to the CPD in which it forms. However, none of these processes can justify an ice loss larger than 9% of the initial ice mass. As established in section 3, the parameter to which the ice fraction is most sensitive to is our initial dust-to-gas ratio in the CPD. For (d/g)=10^{-3}, the solids are dominated by ice (~80wt.% up to ~$110R_{\rm Saturn}$). If these solids formed Titan, a mass of volatiles equivalent to two Titans should be lost either during or post-accretion for Titan to end up with its current ice content, ~30-40wt.%. None of the described ice loss mechanisms can lead to this ice loss, meaning Titan's bulk composition cannot be reconciled with its formation in a CPD with a very low dust-to-gas ratio, (d/g)=10^{-3}.

A high dust-to-gas ratio of $(d/g) = 10^{-1}$ results in a disk saturated in solids, with ~6wt.% of ice. If sufficient ice is to remain in the disk for the formation in Titan with (d/g)=10^{-1}, the ice cannot be directly accreted from the mm-sized particles that carry the bulk of the mass in our grain size distribution. Instead, it must come from captured planetesimals that have ~30-40wt.% of ice.

We find that, for Titan to end up with an ice fraction compatible with MoI observations, the dust-to-gas ratio in the CPD must remain in the order of solar nebula values, (d/g) = O(10^{-2}). In section 5, we found that Titan should have an $f_{\rm ice}$ of 30-40 wt.% in order to match its observed characteristics. If up to a 9% of $f_{\rm ice}$ in the CPD can be lost during or after Titan's accretion, the disk must have an ice mass content of $\sim 30 - 49 wt.\%$. We further constrain the dust-to-gas ratio by investigating a range of $10^{-1.6} - 10^{-2.4}$, and taking into account the possible ice loss mechanisms. The results are shown in Figure 8. To have $f_{\rm ice}$ of $\sim 30 - 49 wt.\%$ in the CPD, the dust-to-gas ratio must be $(d/g) = 10^{-2.05\pm0.2}$, if Titan acquires the bulk of its mass closer than $\sim 100R_{\rm Saturn}$.

Firstly, this supports the fact that Saturn did not open a gap Sasaki et al. (2010). If it had, the dust-to-gas ratio is expected to have decreased significantly by the time of Titan's formation due to dust filtering. While the lower bound, $(d/g) = 10^{-2.25}$, could be compatible with some degree of filtering, it reflects a very generous upper range in CPD ice content, and is unlikely to be representative of CPD conditions upon Titan's accretion.

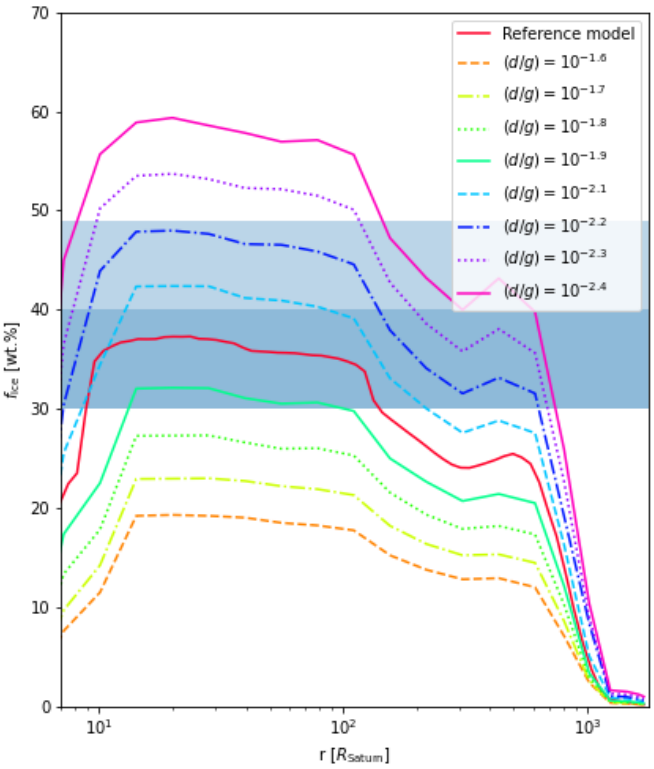

Fig. 8: Column integrated ice over total weight, $f_{\rm ice}$, as a function of distance to Saturn for the reference model (inputs are described in section 2.1), and variations in the dust-to-gas ratio. In blue, the range of $f_{\rm ice}$ that are compatible with the formation of Titan having a MoI of 0.33-0.34. Light blue indicates an $f_{\rm ice}$ in the CPD if ice loss takes place. Dark blue indicates $f_{\rm ice}$ present in Titan's interior.

Secondly, the absence of a gap indicates the main solids delivery mechanism into the CPD can be a direct dust inflow from the PPD; the process of drag capture and ablation of crossing planetesimals is not required to justify Titan's characteristics. Thirdly, defining the volatile availability has implications on the formation of moons other than Titan. If satellites inner to Titan formed from massive rings (Salmon et al. 2010; Canup 2010; Charnoz et al. 2010, 2011; Ćuk et al. 2016), enough ice should be present to result in the rings, whether through the tidal disruption of a Titan-like moon (Canup 2010) or a orbital instability event leading to massive collisions that would create a debris disk (Ćuk et al. 2016).

We conclude that the abundance of ices in the Saturnian CPD is rather insensitive to parameters other than the dust-to-gas ratio. However, a strong background source of UV radiation from the disk's environment ($\chi = 10^4$) or from Saturn ($L_{\rm Saturn} = 10^{-5} L_\odot$) pose a more stringent condition on where Titan can form. These conditions are not expected to represent the disk parameters across the full accretion of Titan, but rather be experienced shortly (as discussed under section 5). Consequently, our CPDs are consistent with the formation of Titan between ~7-$130R_{\rm Saturn}$. The upper bound can be extended to a maximum $r \approx 218R_{\rm Saturn}$ for $\chi = 10^0$, although Titan is unlikely to form at such far distances as accretion is less efficient. The lower bound can be reduced to $r \approx 4R_{\rm Saturn}$ for $L_{\rm Saturn} = 10^{-7} L_\odot$. This reflects a condition that might have taken place during accretion, and is compatible with the rapid orbital expansion of

Titan (Lainey et al. 2020). Owing to the range of CPD conditions that could reproduce a satellite with Titan's characteristics, we sustain that Titan's origin is primordial.

The presence of NH_3 in Saturn's CPD is supported by the identification of the species in the plumes of Enceladus (Waite et al. 2009) and its abundance in comets (i.e. Crovisier 1994). Our CPD models predict that a large NH_3 inventory was available upon Titan's formation. In the reference CPD model, there is more than 15wt.% NH_3 in the ices up to r≈ $28R_{\rm Saturn}$ and more than 10wt.% NH_3 up to $r \approx 111R_{\rm Saturn}$ (as shown in Figure 6). These findings are consistent with the hypothesis that the observed N_2 in Titan is not primordial, but rather was captured as NH_3 (i.e. Niemann et al. 2005). A fraction of NH_3 is expected to have outgassed during accretion and differentiation, to later convert to N_2 by photolysis (Atreya et al. 1978) and shock heating (Jones & Lewis 1987). However, a major fraction of NH_3 remains in the interior (Fortes 2004), which makes the existence of the subsurface ocean possible. We show that Titan is likely to have accreted sufficient NH_3 to possess a subsurface ocean.

Other than NH_3, CH_3OH has been proposed to be a potential antifreeze in Titan's primordial ocean (Deschamps et al. 2010). Our CPD models have yielded insufficient fractions to justify any significant variation in the liquid layer profile for Titan's formation beyond $\sim 11R_{\rm Saturn}$. If Titan formed closer to Saturn than $\sim 11R_{\rm Saturn}$, CH_3OH could be an anti-freeze in Titan's ocean along with NH_3. The large portion of NH_3 in our models, between 10 and 20wt.% in the 10-70$R_{\rm Saturn}$ range with the sole exception of $L_{\rm Saturn} = 10^{-5}L_{\odot}$, yields oceans between 53 to 28 km from the surface, respectively. This is compatible with the possible presence of a conductive layer at 45±15 km discovered by Huygens (Béghin et al. 2010). Our findings thus support the prediction of the existence of a liquid salty layer in Titan.

From radio tracking measurements from Cassini, it can be inferred that the MoI of Titan must be in the range 0.33-0.34 (as discussed in section 4.1). We have established that a sufficient amount of NH_3 is present in Titan to justify the existence of a ~ 300-400 km deep ocean. This ocean decreases the mass being placed in proximity to Titan's surface. Matching a MoI of 0.33-0.34 with an NH_3 ocean generally requires that more than ~ 13wt.% H_2O ice is placed in the core. This is representative of a partially differentiated body, and possibly a core composed of hydrated silicates. Alternatively, the MoI can be reached if the ocean's density is large (~1200 kg m^{-3}). Consequently, our CPD models favor a scenario in which Titan has either an H_2O ice content higher than 13wt.% in its core or an ocean enriched in antifreeze compounds denser than NH_3.

7. Conclusions

We have evaluated a ensemble of CPDs in their capacity to form a moon with Titan's ice to rock fraction, mean density and radius, as well as its MoI, and concluded that:

1. To form a moon with Titan's bulk ice content, the dust-to-gas ratio in the CPD must be $(d/g) = 10^{-2.05\pm0.2}$, if Titan acquires the bulk of its mass closer than $\sim 100R_{\rm Saturn}$. The ice availability upon accretion is otherwise inconsistent with Titan's MoI.
2. A large NH_3 reservoir was available upon Titan's formation, of the order of 10-20wt.% of the total nebular volatile mass from 10 to 70 $R_{\rm Saturn}$ for all CPD models except the one with a very luminous Saturn, $L_{\rm Saturn} = 10^{-5}L_{\odot}$. This is consistent with the hypothesis that the observed N_2 in Titan is captured as NH_3 and converted by photolysis (Atreya et al. 1978) and shock heating (Jones & Lewis 1987).
3. The NH_3 inventory in the CPD is compatible with the possible presence of a conductive layer at 45±15 km depth as revealed by the Huygens probe (Béghin et al. 2010).
4. Our CPD models are reconcilable with the formation of Titan in close proximity to Saturn ($r \geq 7R_{\rm Saturn}$). Formation at $\sim 5R_{\rm Saturn}$, which agrees with the rapid orbital expansion of Titan in the resonant locking scenario (Lainey et al. 2020), requires $L_{\rm Saturn} = 10^{-7}L_{\odot}$.

References

Alibert, Y. & Mousis, O. 2007, Astronomy and Astrophysics, 465
Alibert, Y., Mousis, O., & Benz, W. 2005, Astronomy and Astrophysics [arXiv:0505367]
Anderson, S. E., Mousis, O., & Ronnet, T. 2021, The Planetary Science Journal [arXiv:2102.03230]
Archinal, B. A., Acton, C. H., A'Hearn, M. F., et al. 2018, Celestial Mechanics and Dynamical Astronomy, 130
Atreya, S. K., Donahue, T. M., & Kuhn, W. R. 1978, Science, 201
Bierson, C. J. & Nimmo, F. 2020, The Astrophysical Journal, 897
Birnstiel, T., Klahr, H., & Ercolano, B. 2012, Astronomy and Astrophysics [arXiv:1201.5781]
Brian Tonks, W. & Jay Melosh, H. 1992, Icarus, 100
Burrows, A., Marley, M., Hubbard, W. B., et al. 1997, The Astrophysical Journal [arXiv:9705201]
Béghin, C., Sotin, C., & Hamelin, M. 2010, Comptes Rendus Geoscience, 342, 425
Canup, R. M. 2010, Nature
Canup, R. M. & Ward, W. R. 2002, The Astronomical Journal
Canup, R. M. & Ward, W. R. 2006, Nature
Castillo-Rogez, J., Johnson, T. V., Lee, M. H., et al. 2009, Icarus, 204, 658
Castillo-Rogez, J. C. & Lunine, J. I. 2010, Geophysical Research Letters
Charnoz, S., Crida, A., Castillo-Rogez, J. C., et al. 2011, Icarus
Charnoz, S., Morbidelli, A., Dones, L., & Salmon, J. 2009, Icarus
Charnoz, S., Salmon, J., & Crida, A. 2010, Nature
Cilibrasi, M., Szulágyi, J., Mayer, L., et al. 2018, Monthly Notices of the Royal Astronomical Society [arXiv:1801.06094]
Crida, A. & Morbidelli, A. 2007, Monthly Notices of the Royal Astronomical Society [arXiv:0703151]
Crovisier, J. 1994, Symposium - International Astronomical Union, 160
Ćuk, M., Dones, L., & Nesvorný, D. 2016, The Astrophysical Journal
Cuppen, H. M. & Herbst, E. 2007, The Astrophysical Journal, 668
D'Alessio, P., Canto, J., Calvet, N., & Lizano, S. 1998, The Astrophysical Journal [arXiv:9806060]
Deschamps, F., Mousis, O., Sanchez-Valle, C., & Lunine, J. I. 2010, Astrophysical Journal, 724
Draine, B. T. 2006, The Astrophysical Journal [arXiv:0507292]
Dubrulle, B., Morfill, G., & Sterzik, M. 1995, Icarus
Dwyer, C. A., Nimmo, F., Ogihara, M., & Ida, S. 2013, Icarus, 225
Estrada, P. R. & Mosqueira, I. 2006, Icarus, 181, 486
Estrada, P. R., Mosqueira, I., Lissauer, J. J., D'Angelo, G., & Cruikshank, D. P. 2017, in Europa
Fortes, A. 2004, Earth
Fortes, A. D. 2012, in Planetary and Space Science
Fortes, A. D., Grindrod, P. M., Trickett, S. K., & Vočadlo, L. 2007, Icarus
Fujii, Y. I. & Ogihara, M. 2020, Astronomy and Astrophysics
Fujii, Y. I., Okuzumi, S., Tanigawa, T., & Inutsuka, S. I. 2014, Astrophysical Journal [arXiv:1402.6091]
Gao, P. & Stevenson, D. J. 2013, Icarus
Gautier, D. & Raulin, F. 1997, in ESA Special Publication, Vol. 1177, Huygens: Science, Payload and Mission, ed. A. Wilson, 359
Grasset, O., Sotin, C., & Deschamps, F. 2000, Planetary and Space Science
Habing, H. J. 1968, Bull. Astron. Inst. Netherlands
Hallam, P. D. & Paardekooper, S.-J. 2017, Monthly Notices of the Royal Astronomical Society [arXiv:1705.07528]
Hamilton, D. P. 2013, in AAS/Division for Planetary Sciences Meeting Abstracts, Vol. 45, AAS/Division for Planetary Sciences Meeting Abstracts #45, 302.01
Hammond, N. P., Parmenteir, E. M., & Barr, A. C. 2018, Journal of Geophysical Research: Planets, 123
Hartung, M., Herbst, T. M., Dumas, C., & Coustenis, A. 2006, Journal of Geophysical Research E: Planets, 111
Ida, S. 2019, The origin of Saturn's rings and moons
Iess, L., Militzer, B., Kaspi, Y., et al. 2019, Science
Iess, L., Rappaport, N. J., Jacobson, R. A., et al. 2010, Science

Jacobson, R., Antreasian, P., Bordi, J., et al. 2006, The Astronomical Journal
Jones, T. D. & Lewis, J. S. 1987, Icarus, 72
Kamp, I., Thi, W. F., Woitke, P., et al. 2017, Astronomy and Astrophysics, 607
Kamp, I., Tilling, I., Woitke, P., Thi, W. F., & Hogerheijde, M. 2010, Astronomy and Astrophysics, 510
Kronrod, V. & Makalkin, A. 2017, Capture of bodies into the circumplanetary disks of young Jupiter and Saturn.
Lainey, V., Casajus, L. G., Fuller, J., et al. 2020, Nature Astronomy
Lambrechts, M., Johansen, A., & Morbidelli, A. 2014, Astronomy and Astrophysics [arXiv:1408.6087]
Lissauer, J. J., Hubickyj, O., D'Angelo, G., & Bodenheimer, P. 2009, Icarus [arXiv:0810.5186]
Liu, B. & Ormel, C. W. 2018, Astronomy and Astrophysics [arXiv:1803.06149]
Lodders, K. 2003, The Astrophysical Journal
Lubow, S. H., Seibert, M., & Artymowicz, P. 1999, The Astrophysical Journal [arXiv:9910404]
Lunine, J., Choukroun, M., Stevenson, D., & Tobie, G. 2010, in Titan from Cassini-Huygens
Lunine, J. I. & Stevenson, D. J. 1982, Icarus
Makalkin, A. B. & Dorofeeva, V. A. 2006, Solar System Research
Martin, R. G. & Lubow, S. H. 2011, Monthly Notices of the Royal Astronomical Society
Mathis, J. S., Rumpl, W., & Nordsieck, K. H. 1977, The Astrophysical Journal, 217
McElroy, D., Walsh, C., Markwick, A. J., et al. 2013, Astronomy and Astrophysics, 550
Miguel, Y. & Ida, S. 2016, Icarus
Mosqueira, I. & Estrada, P. R. 2003, Icarus
Mumma, M. J. & Charnley, S. B. 2011, Annual Review of Astronomy and Astrophysics, 49
Niemann, H. B., Atreya, S. K., Bauer, S. J., et al. 2005, Nature
Niemann, H. B., Atreya, S. K., Demick, J. E., et al. 2010, Journal of Geophysical Research E: Planets
Nimmo, F. & Korycansky, D. G. 2012, Icarus, 219
Oberg, N. 2021, (personal communication)
Oberg, N., Kamp, I., Cazaux, S., & Rab, C. 2020, Astronomy & Astrophysics
Ormel, C. W. 2017
Ormel, C. W. & Liu, B. 2018, Astronomy and Astrophysics [arXiv:1803.06150]
Owen, T., Mahaffy, P., Niemann, H. B., et al. 1999, Nature
Pepin, R. O. 1992, Annual review of Earth and planetary sciences. Vol. 20
Phillips, M. W., Tremblin, P., Baraffe, I., et al. 2020, Astronomy and Astrophysics [arXiv:2003.13717]
Pollack, J. B., Grossman, A. S., Moore, R., & Graboske, H. C. 1977, Icarus
Quillen, A. C. & Trilling, D. E. 1998, The Astrophysical Journal
Ribas, I., Guinan, E. F., Gudel, M., & Audard, M. 2005, The Astrophysical Journal [arXiv:0412253]
Ronnet, T. & Johansen, A. 2019, Capture and ablation of planetesimals as foundation for a pebble accretion scenario
Salmon, J., Charnoz, S., Crida, A., & Brahic, A. 2010, Icarus
Sasaki, T., Stewart, G. R., & Ida, S. 2010, Astrophysical Journal
Serman, M. 2019
Shakura, N. I. & Sunyaev, R. A. 1973, Symposium - International Astronomical Union
Shibaike, Y., Ormel, C. W., Ida, S., Okuzumi, S., & Sasaki, T. 2019, The galilean satellites formed slowly from pebbles
Shu, F. H., Johnstone, D., & Hollenbach, D. 1993, Icarus, 106
Solomonidou, A., Neish, C., Coustenis, A., et al. 2020, Astronomy and Astrophysics, 641
Sotin, C., Grasset, O., & Beauchesne, S. 1998
Tobie, G., Gautier, D., & Hersant, F. 2012, Astrophysical Journal
Tobie, G., Grasset, O., Lunine, J. I., Mocquet, A., & Sotin, C. 2005, Icarus
Tobie, G., Lunine, J., Monteux, J., Mousis, O., & Nimmo, F. 2014, The origin and evolution of Titan, 29–62
Ulmer, P. & Trommsdorff, V. 1995, Science, 268
Waite, J. H., Glein, C. R., Perryman, R. S., et al. 2017, Science, 356
Waite, J. H., Lewis, W. S., Magee, B. A., et al. 2009, Nature, 460
Woitke, P. 2015, in EPJ Web of Conferences
Woitke, P., Kamp, I., & -F. Thi, W. 2009, Astronomy and Astrophysics
Woitke, P., Min, M., Pinte, C., et al. 2016, Astronomy and Astrophysics [arXiv:1511.03431]
Woitke, P., Riaz, B., Duchêne, G., et al. 2011, Astronomy and Astrophysics
Youdin, A. N. & Lithwick, Y. 2007, Icarus [arXiv:0707.2975]
Zebker, H. A., Stiles, B., Hensley, S., et al. 2009, Science, 324
Zolotov, M., Owen, T., Atreya, S., Niemann, H., & Shock, E. 2005, AGU Fall Meeting Abstracts, -1, 04

Appendix A: Circumplanetary disk characteristics

The dependence of the main chemical species on the input parameters $\dot{M}$ and $T_{\rm back}$ are shown in Figure A.1. It can be seen that $\dot{M}$ has a negligible impact on the species abundances. This is also the case for a background temperature $T_{\rm back}$ between 20-40 K. We show the effects of further increasing $T_{\rm back}$ to 50 K. While this changes the carbon-bearing species, H_2O+OH and NH_3 have a negligible change for $r < 100 R_{\rm Saturn}$. Even if $T_{\rm back} = 50$ K upon Titan's formation, our findings do not vary as they focus on H_2O+OH and NH_3.

The oxygen, nitrogen and carbon elemental ice fractions in the ices for the CPD reference model are shown in Figure A.2. The mid-plane temperature profiles and main chemical species are shown as a function of distance to Saturn in Figure A.3 and Figure A.4 for the considered CPDs. We provide a description of the CPDs in section 2.

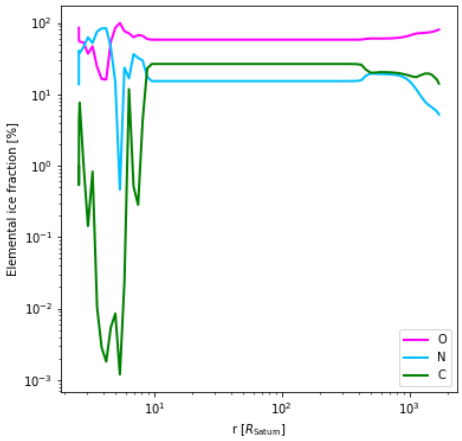

Fig. A.2: Oxygen, nitrogen and carbon elemental ice fractions in the ices for the CPD reference model as a function of r. A description of the CPD characteristics is given in section 2.1.

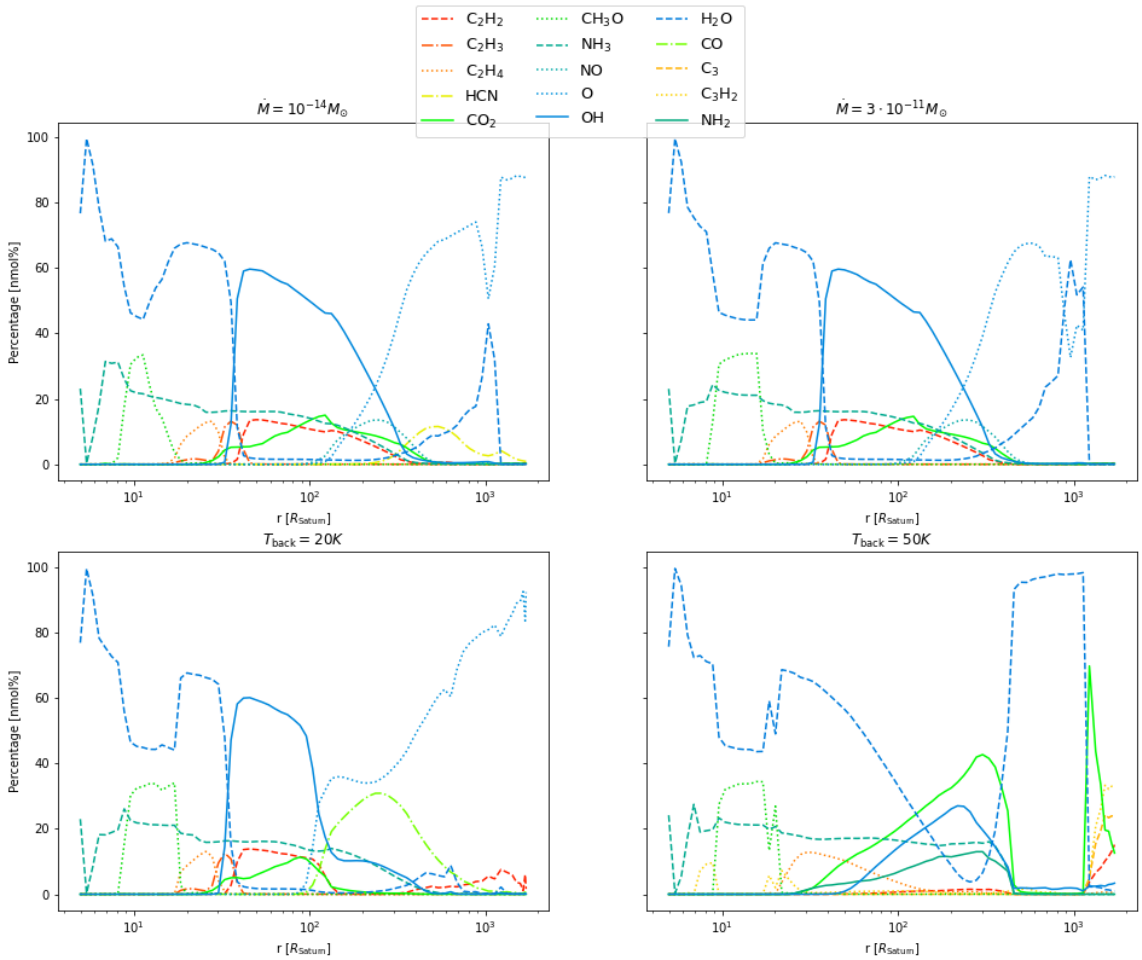

Fig. A.1: Chemical species abundances (column integrated) for varied parameters in $\dot{M}$ and $T_{\rm back}$, as a function of r. We discuss the input parameters in section 2. Only species reaching more than a 5% molecular abundance across two consecutive grid points are presented.

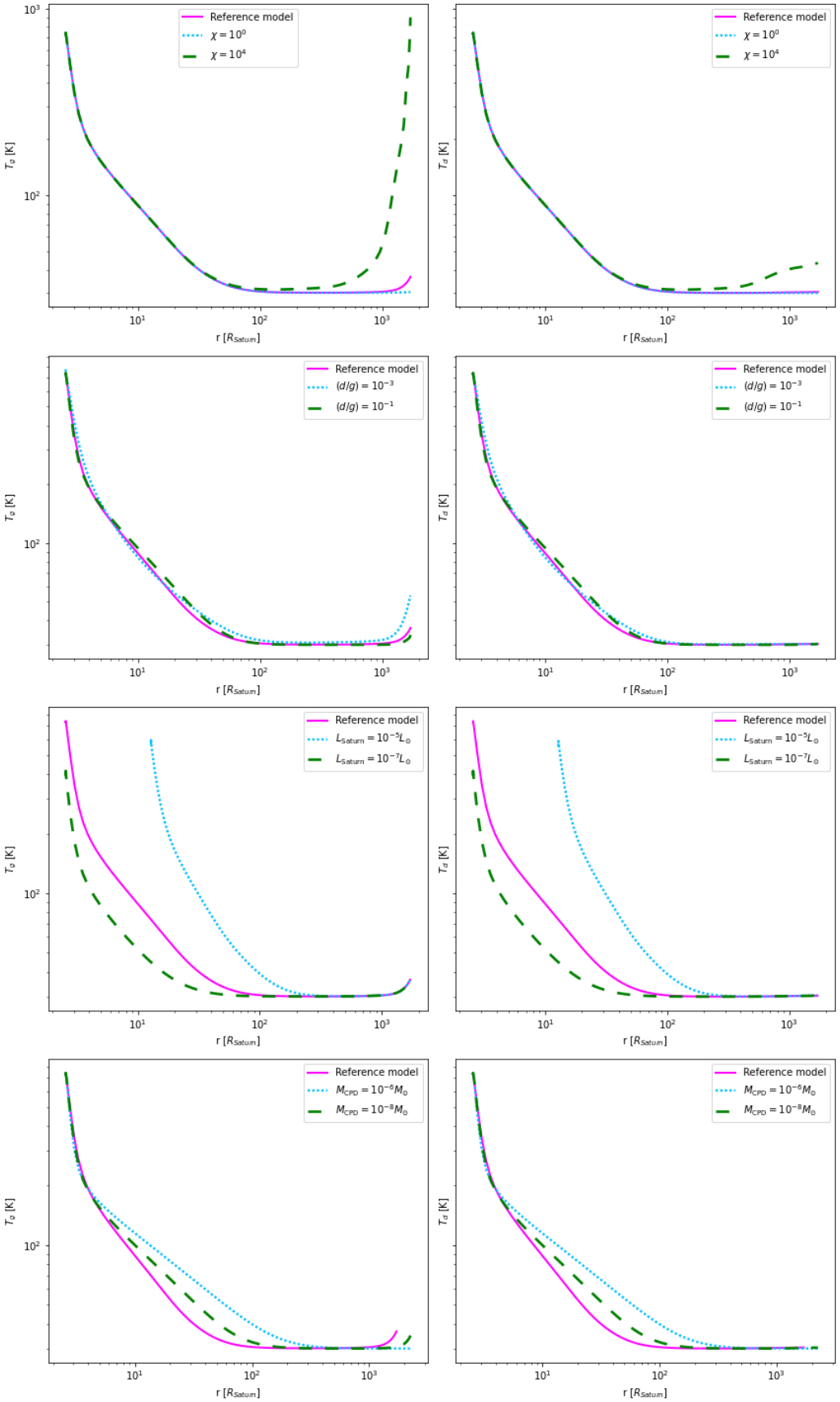

Fig. A.3: Mid-plane temperature profiles for the gas (left) and the dust (right) for the reference model (in magenta) and the varied parameters, as a function of r. The input parameters are described in section 2.

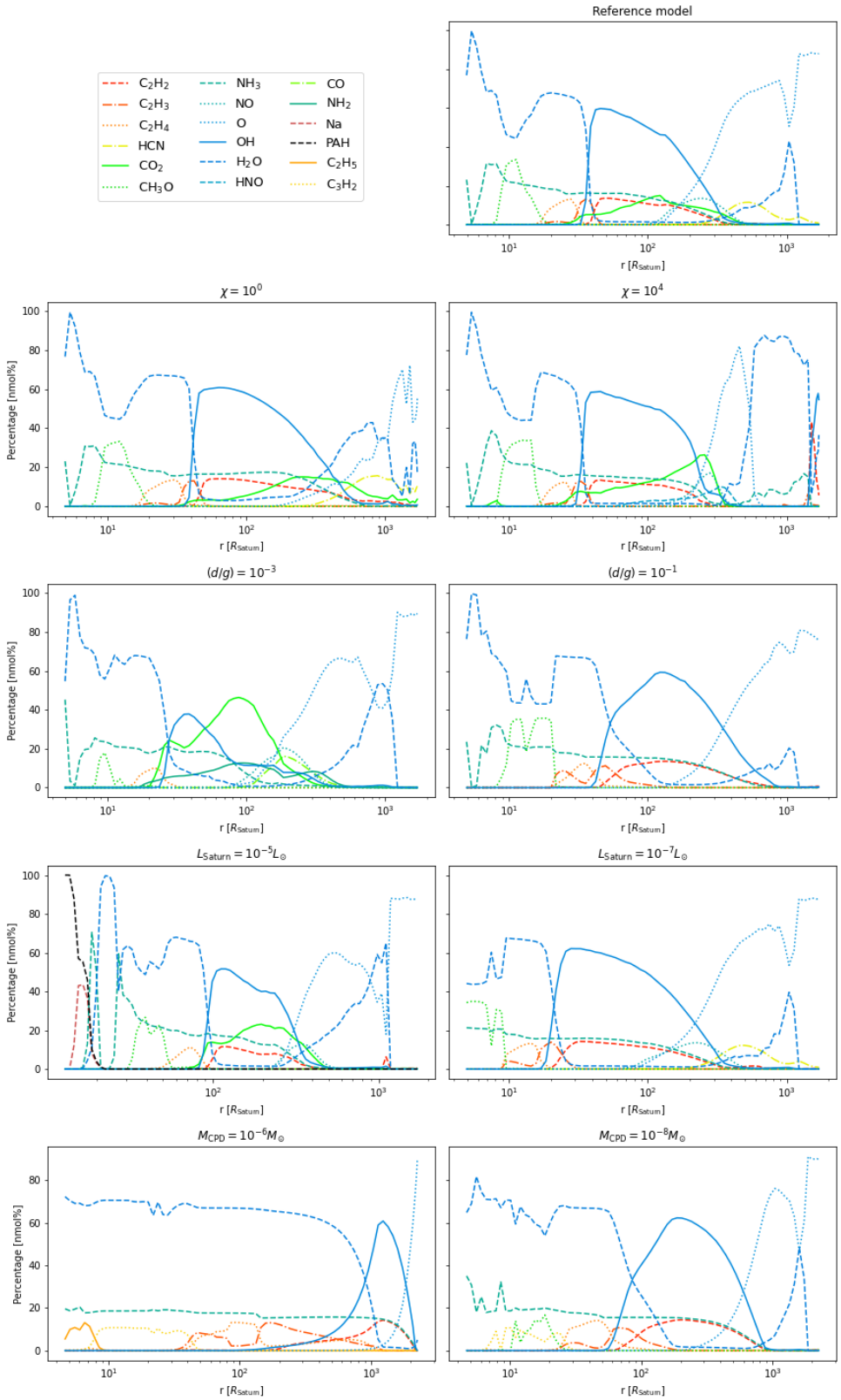

Fig. A.4: Chemical species abundances (column integrated) for the reference model and the varied parameters, as a function of r. We discuss the input parameters in section 2. Only species reaching more than a 5% molecular abundance across two consecutive grid points are presented.

Appendix B: Interior model profiles

Interior models are detailed at Titan's present location ($r \approx 21 R_{\mathrm{Saturn}}$) in Figure 5, Figure B.1 and Figure B.2, and a description of the physical parameters can be found in Table B.1. Resulting core densities in the anhydrous core case are compatible with the density of San Carlos Olivine at low pressure conditions (ρ_{core} = 3343 kg m^{-3}). The hydrated silicate cores have densities closer to that of antigorie at low pressures (ρ_{core} = 2558 kg m^{-3}) (Fortes 2004). At this location, only the dense ocean case complies with the constraints described under section 4.1.

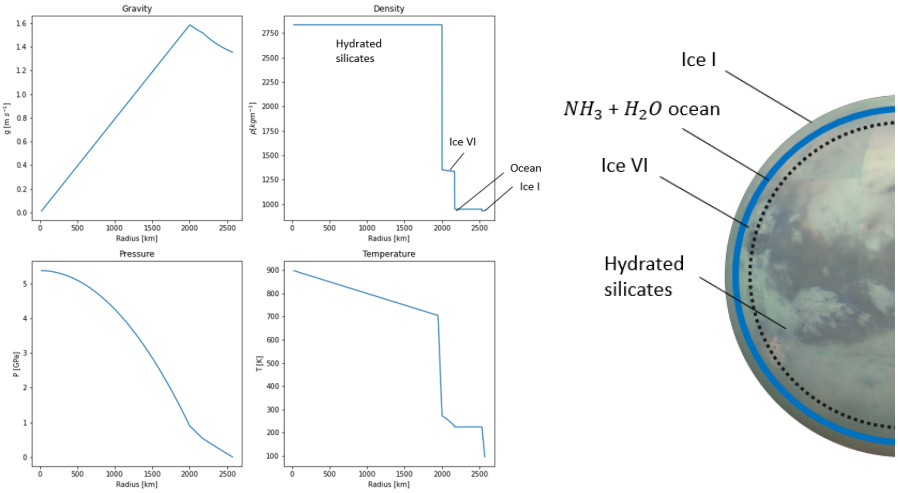

Fig. B.1: Model characteristics for an ice bearing core and an ammonia rich ocean in Titan. On the left, profiles of gravity, density, pressure and temperature inside Titan are shown for in-situ formation at the moon's present location in the reference model (f_{ice}=37wt.% and 16wt.% NH_3 over ice weight). On the right, a depiction of the modelled layers is provided (not to scale). Titan image credit: NASA/JPL/University of Arizona/University of Idaho.

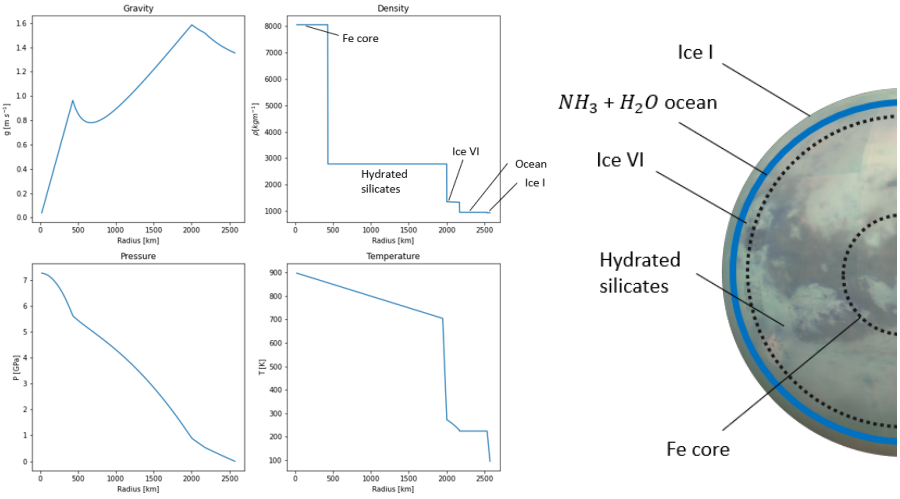

Fig. B.2: Model characteristics for a differentiated core, composed by pure Fe surrounded by hydrated silicates (or possibly an undifferentiated outer core). The icy layer contains an ammonia rich ocean. On the left, profiles of gravity, density, pressure and temperature inside Titan are shown for in-situ formation at the moon's present location in the reference model (37wt.% of ice and 16wt.% NH_3 over ice weight). On the right, a depiction of the modelled layers is provided (not to scale). Titan image credit: NASA/JPL/University of Arizona/University of Idaho.

Table B.1: Numerical results for interior models at Titan's present location in reference model.

Description	MoI	ρ_{core} [kg m^{-3}]	R_{core} [km]	Ocean depth [km]	Ocean extent [km]	
Anhydrous silicate core	0.312	3349.467	1818.701	36.000	370.039	Figure 5
Hydrated/undifferentiated core	0.327	2840.683	2001.268	36.000	370.039	Figure B.1
Hydrated/undifferentiated outer core with pure Fe inner core	0.323	8058.300, 2788.264	430.391, 2001.268	36.000	370.039	Figure B.2
Hydrated/undifferentiated core with dense ocean	0.336	2690.894	2037.733	36.000	370.039	-

Appendix C: Migration

We assess the effect of migration on the bulk composition of Titan. To that end, we assume Titan grows through pebble accretion from an initial seed mass. We compute the pebble accretion efficiency as a function of distance to Saturn and seed mass in section C.1. In section C.2, we impose different migration tracks, and let Titan grow at a rate depending on the pebble accretion efficiency. The effect of migration on Titan's bulk chemistry is discussed under section C.3.

Appendix C.1: Pebble accretion efficiency

In this study, the formation or capture of the seed itself is not considered. We form Titan in the CPD models from an initial (spherical) seed radius ~130 km, corresponding to Titan's mean density and a seed to planet mass ratio of $q_s = 10^{-7.5}$. We investigate its further growth via the pebble accretion mechanism, by which small particles of negligible gravitational mass compared to the seed are accreted onto the growing body (see Ormel 2017; Ormel & Liu 2018; Liu & Ormel 2018; Lambrechts et al. 2014).

We compute the pebble accretion efficiency $\epsilon_{\rm PA}$ as a function of distance to Saturn and seed mass in our reference CPD model. This efficiency refers to the probability that a pebble, drifting to the central body (i.e. Saturn) is accreted by the minor forming body (i.e. Titan) (Ormel & Liu 2018). The values of $\epsilon_{\rm PA}$ are computed following the framework provided in Ormel & Liu (2018) and Liu & Ormel (2018), with the characteristics of the CPD reference model described in section 2.1. Ormel & Liu (2018) and Liu & Ormel (2018) carry out three body –central, minor body and pebble– integrations to follow the drifting trajectory of pebbles in a PPD. They provide analytical fits describing $\epsilon_{\rm PA}$ in terms of growing body, disk and pebble properties, applicable in the $10^{-3} \leq \tau_s < 1$ range, where $\tau_{\rm s}$ is the pebble dimensionless stopping time.

The expression for $\epsilon_{\rm PA}$ is a combination of the 2D and 3D limits. In the former (2D), all pebbles reside in the midplane. In the latter (3D), turbulence stirring pebbles out of the midplane –and increasing relative velocities– is accounted for. The total accretion efficiency then follows from combination of both regimes, $\epsilon_{\rm 2D}$ and $\epsilon_{\rm 3D}$ (Ormel & Liu 2018),

$$\epsilon_{\rm PA} = (\epsilon_{\rm 2D}^{-2} + \epsilon_{\rm 3D}^{-2})^{-1/2}. \tag{C.1}$$

When the pebble accretion radius exceeds the pebble scale height, $h_{\rm p}$, the first term dominates. This value is obtained from the analytical approximation (Youdin & Lithwick 2007),

$$h_{\rm p} = h_{\rm g}\left(1 + \frac{\tau_{\rm s}}{\alpha}\frac{1+2\tau_{\rm s}}{1+\tau_{\rm s}}\right)^{-1/2}. \tag{C.2}$$

In the planar approximation (2D), accretion efficiency is divided into two terms, $\epsilon_{\rm 2D} = \epsilon_{\rm 2D,set} + \epsilon_{\rm 2D,bal}$.

The first term, $\epsilon_{\rm 2D,set}$, refers to the settling regime where the gas-drag effect is relevant. The second term $\epsilon_{\rm 2D,bal}$, refers to the ballistic regime, where gas-drag is insufficient for the capture of pebbles and accretion can only take place upon impact of pebbles on the growing satellite's surface. These two terms follow Equation C.3 and Equation C.4, respectively,

$$\epsilon_{\rm 2D,set} = 0.32\sqrt{\frac{q_{\rm s}}{\eta^2\tau_{\rm s}}\frac{\Delta v}{v_{\rm K}}}f_{\rm set}, \tag{C.3}$$

$$\epsilon_{\rm 2D,bal} = \frac{r_{\rm s}}{2\pi\tau_{\rm s}\eta r}\sqrt{\frac{2q_{\rm s}r}{r_{\rm s}} + \left(\frac{\Delta v}{v_{\rm K}}\right)^2}(1 - f_{\rm set}), \tag{C.4}$$

where $v_{\rm K}$ is the Keplerian speed, $r_{\rm s}$ is the seed radius and η is the headwind prefactor,

$$\eta = -\frac{1}{2}\frac{H_{\rm g}^2}{r^2}\frac{\delta log P_{\rm g}}{\delta log r}, \tag{C.5}$$

with $P_{\rm g}$ the gas pressure in the midplane. Assuming the satellite is in a circular orbit, the relative velocity between the satellite and the pebble is given by,

$$\Delta v = \left[1 + 5.7\left(\frac{q_{\rm s}}{q_{\rm hw/sh}}\right)\right]^{-1} v_{\rm hw} + v_{\rm sh}, \tag{C.6}$$

where $v_{\rm hw} = \eta v_{\rm K}$ is the headwind velocity experienced by particles, $v_{\rm sh} = 0.52(q_{\rm s}\tau_{\rm s})^{1/3}v_{\rm K}$ is the Keplerian shear velocity between the satellite and the pebble and $q_{\rm hw/sh} = \eta^3/\tau_{\rm s}$ is the transition mass ratio between the headwind and shear regimes (Liu & Ormel 2018). In Equation C.4 and Equation C.3, $f_{\rm set} = exp[-0.5(\Delta v/v_*)^2]$ is a modulation factor, with $v_* = (q_{\rm s}/\tau_{\rm s})^{1/3}v_{\rm K}$ the transition velocity between both regimes (Liu & Ormel 2018).

Similarly to the 2D limit, in the 3D regime (Ormel & Liu 2018; Liu & Ormel 2018), $\epsilon_{\rm 3D} = \epsilon_{\rm 3D,set} + \epsilon_{\rm 3D,bal}$,

$$\epsilon_{\rm 3D,set} = 0.39\frac{q_{\rm s}}{\eta h_{\rm p}}f_{\rm set}^2, \tag{C.7}$$

$$\epsilon_{\rm 3D,bal} = \frac{1}{4\sqrt{2\pi}\eta\tau_{\rm s}h_{\rm p}}\left(2q_{\rm s}\frac{v_{\rm k}}{\Delta v}\frac{r_{\rm s}}{r} + \left(\frac{r_{\rm s}}{r}\right)^2\frac{\Delta v}{v_{\rm k}}\right)(1 - f_{set}^2), \tag{C.8}$$

We solve Equation C.1 to find $\epsilon_{\rm PA}$ for every seed mass ratio $q_{\rm s}$ and distance to Saturn r, shown in Figure C.1. We observe $\epsilon_{\rm PA}$ increases towards Saturn, for higher seed masses. The top left area, in yellow, corresponds to the most efficient accretion.

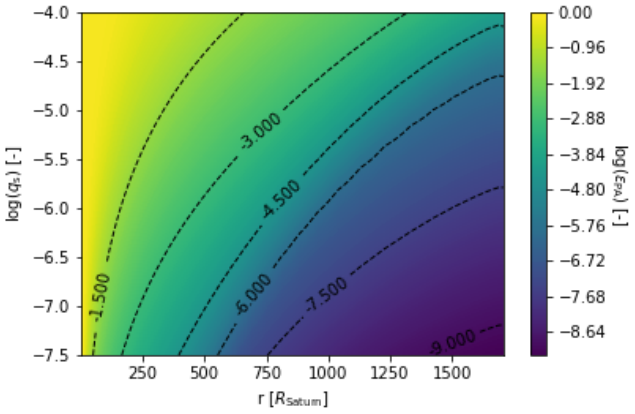

Fig. C.1: Pebble accretion efficiency in the reference model (see section 2.1) as a function of r, and seed to planet mass, $q_{\rm s}$. Results are shown for an assumed $\tau_{\rm s} = 5 \cdot 10^{-3}$, and a seed mass up to Titan's current mass, $q_{\rm s} \approx 10^{-4} \approx M_{\rm Titan}/M_{\rm Saturn}$.

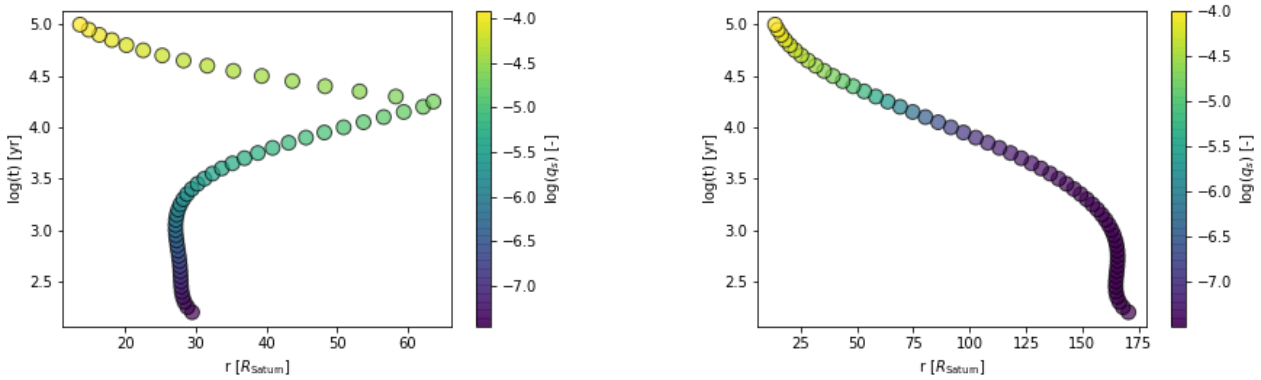

(a) Migration track 'M1'.

(b) Migration track 'M2'.

Fig. C.2: Cumulative mass of Titan as a function of its migration track across time, for migration scenarios (a) 'M1' and (b) 'M2'. The position of Titan as a function of time is taken from Fujii & Ogihara (2020). The growth of the seed at each timestep is computed from Equation C.9.

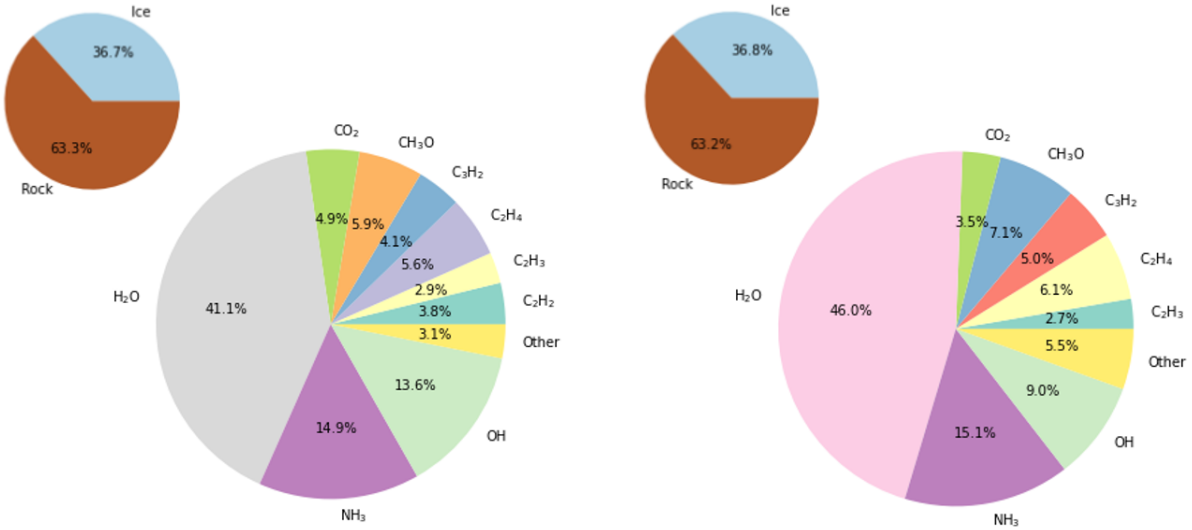

(a) Bulk composition in 'M1' scenario.

(b) Bulk composition in 'M2' scenario.

Fig. C.3: Rock-to-ice and ices bulk composition for Titan finishing its growth at $r \approx 13.6 R_{\rm Saturn}$ in the reference model with (a) 'M1' migration and (b) 'M2' migration. The bulk composition acquired at each radial distance is proportional to the mass increase depicted in Figure C.2.

Appendix C.2: Migration tracks

We subject the seed to two boundary migration tracks computed in Fujii & Ogihara (2020) for $\alpha = 10^{-4}$. The tracks in Fujii & Ogihara (2020) describe the orbital evolution since the disk starts to dissipate. We assume Titan grows throughout these from $q_{\rm s} = 10^{-7.5}$ to its present mass, $q_{\rm s} \approx 10^{-4}$, to get a first estimate of the effect of migration on the moon's bulk chemistry. In future work, the migration track should be self-consistent with the moon's mass growth, rather than imposed.

Having the seed position as a function of time, $r(t)$, we compute the mass increase through,

$$q_{\rm s}(t+1) = q_{\rm s}(t) + \dot{M}\epsilon_{PA}(q_{\rm s}(t), r(t)), \tag{C.9}$$

for the two considered tracks, named 'M1' and 'M2'. The former is the closest initial location allowing for Titan's survival in Fujii & Ogihara (2020), while the latter reflects an extended inwards migration. These are shown in Figure C.2, along with the total seed mass at each radial position. The color in the figures reflects the cumulative seed mass. Dark purple indicates the initial seed mass, $q_{\rm s} = 10^{-7.5}$, and yellow reflects the highest seed masses, as Titan approaches its final location. These seed masses are indicated in the right color bar in Figure C.2. In both migration scenarios, ~50% of Titan's mass is acquired in at $r \leq 21 R_{\rm Saturn}$, corresponding to the last five yellow dots in Figure C.2. This is caused by the increased $\epsilon_{\rm PA}$ both for higher mass seeds and reduced radial distance to Saturn (yellow values in Figure C.1), which triggers a fast growth in the last migration stages.

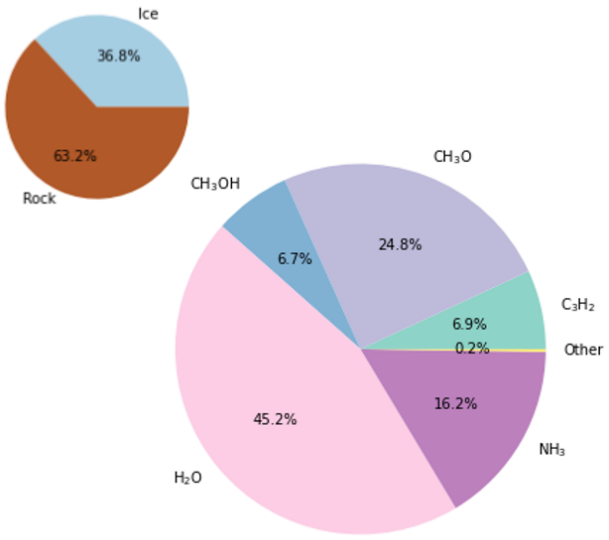

Fig. C.4: Rock-to-ice and ices bulk composition for Titan forming in-situ at $r \approx 13.6 R_{\rm Saturn}$ in the reference model.

Appendix C.3: Effect of migration on bulk chemistry

The body's bulk composition might be dependant on radial mixing, and consist of an amalgam of the solids with different chemical composition that are present at different radii. As shown in Figure A.4, we know the abundance of each icy species as a function of distance to Saturn. From Figure C.2, we know how much mass Titan acquires at each radial location. We thus compute the final bulk composition corresponding to the mass growth in the 'M1' and 'M2' migration scenarios. Figure C.3 shows the rock-to-ice in Titan's interior (small pie plots) and the main ice species (big pie plots) in Titan, resulting from the radial mixing introduced by migration. For both migration tracks, water content, H_2O+OH, is dominant, being 54-55wt.% of the total ices and the NH_3 content is $\sim 15 wt.\%$.

In section C.2, we find that Titan acquires the bulk of its mass as it nears its final location. Similarly, ~50% of Titan's composition is acquired within $< 10 R_{\rm Saturn}$ from its final position in the CPD. This implies $\leq 5\%$ difference in icy species abundance for the 'M1' and 'M2' scenarios, despite the differences between the tracks. This difference is further reduced for species with stable abundances throughout the disk. This is the case of NH_3 (see section 3), for which it is $\pm O(10^{-3})$. Similarly, the ice-to-rock ratio is close to constant, as described under section 3, and only varies within $\pm O(10^{-3})$ for the different migration tracks.

We compare the final bulk composition in the 'M1' and 'M2' scenarios to that of a formation in-situ at the final location, shown in Figure C.4. The major difference resides in the variety of C-bearing species. Their increased diversity in outer radii is reflected in Figure C.3. In the in-situ case, formation occurs before the snowlines for CO_2, C_2H_2, C_2H_3 and C_2H_4. The total C elemental fraction is comparable in the in-situ, 'M1' and 'M2' scenarios; it is close to constant after $r = 10 R_{\rm Saturn}$, as are the N and O fractions (as shown in Figure A.2).

We conclude that the elemental fractions for a migrating Titan do not vary with respect to in-situ formation, but migration can introduce a larger diversity in species. Furthermore, the bulk composition is mostly sensitive to the final location, not the migration track. However, it remains unknown where the body finished accreting. Titan could have ceased to migrate upon reaching its current location (Fujii & Ogihara 2020) or in proximity to Saturn, only to later migrate outwards by interaction with the planet (Lainey et al. 2020). Narrowing down the migration path could help in refining our interior models, and the assessment of species other than NH_3 and H_2O.

Appendix D: Verification and validation

Appendix D.1: Disk models

We model a TTauri PPD, so as to compare our Spectral Energy Distribution (SED) output to that provided in (Serman 2019). The results, shown under Figure D.1, serve as a way to test ProDiMo before adapting it to model the Saturnian CPD.

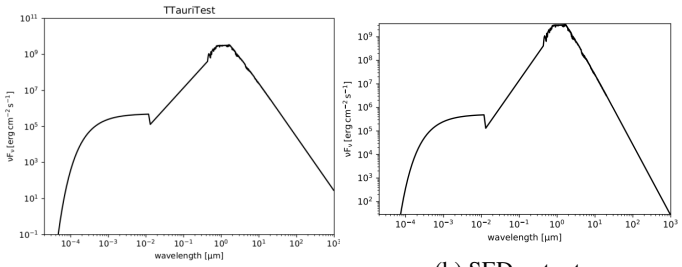

(a) SED in Serman (2019)

(b) SED output.

Fig. D.1: Comparison of spectrum of a TTauri star as described in Serman (2019) with our own ProDiMo results.

Our best models are consistent with the hypothesis that Saturn did not open a gap in the CPD. This is also considered when selecting the input background temperature and dust sizes for the disks (see section 2.1 for a discussion). We verify this lack of a gap analytically. Gap opening occurs since the torque exerted by the planet on the surrounding disk overcomes the disc's viscous torque trying to fill the gap region. Besides this viscous condition, a condition for a gap to open is the thermal criterion: the planet's Hill radius must be larger than the disk scale height such that angular momentum is deposited in the proximity of the planet (Hallam & Paardekooper 2017). More particularly, gap opening occurs for a gap opening parameter $\mathcal{P} \leq 1$,

$$\mathcal{P} = \frac{3}{4}\frac{H_g}{r_H} + \frac{50}{M_{\rm Saturn}\mathcal{R}} = \frac{h_g(a_{\rm Saturn})}{M_{\rm Saturn}^{1/3}} + \frac{50\alpha h_g(a_{\rm Saturn})^2}{M_{\rm Saturn}}, \qquad \text{(D.1)}$$

with $\mathcal{R}$ the Reynolds number (Canup & Ward 2002; Crida & Morbidelli 2007). With $\alpha = 10^{-3}$, $h_g(a) = 1.88$ and $M_{\rm Saturn} = 2.858 \cdot 10^{-4} M_\odot$, we obtain $\mathcal{P} = 647.53$. Therefore, the gap opening criterion is not satisfied and we have verified that Saturn does not open a gap.

Appendix D.2: Interior models

The ice I shell thickness is determined such that it matches the global heat flux expelled from the core. We verify the correctness of our heat flux computations as a function of shell thickness. We contrast our output to that of Grasset et al. (2000), for 5wt.% and 15wt.% NH_3. The results are shown in Figure D.4. The higher the ammonia abundance, the more sensitive the heat flux is to the pressure and temperature rounding errors. This is reflected in the larger error in the 15wt.% NH_3 case (bottom

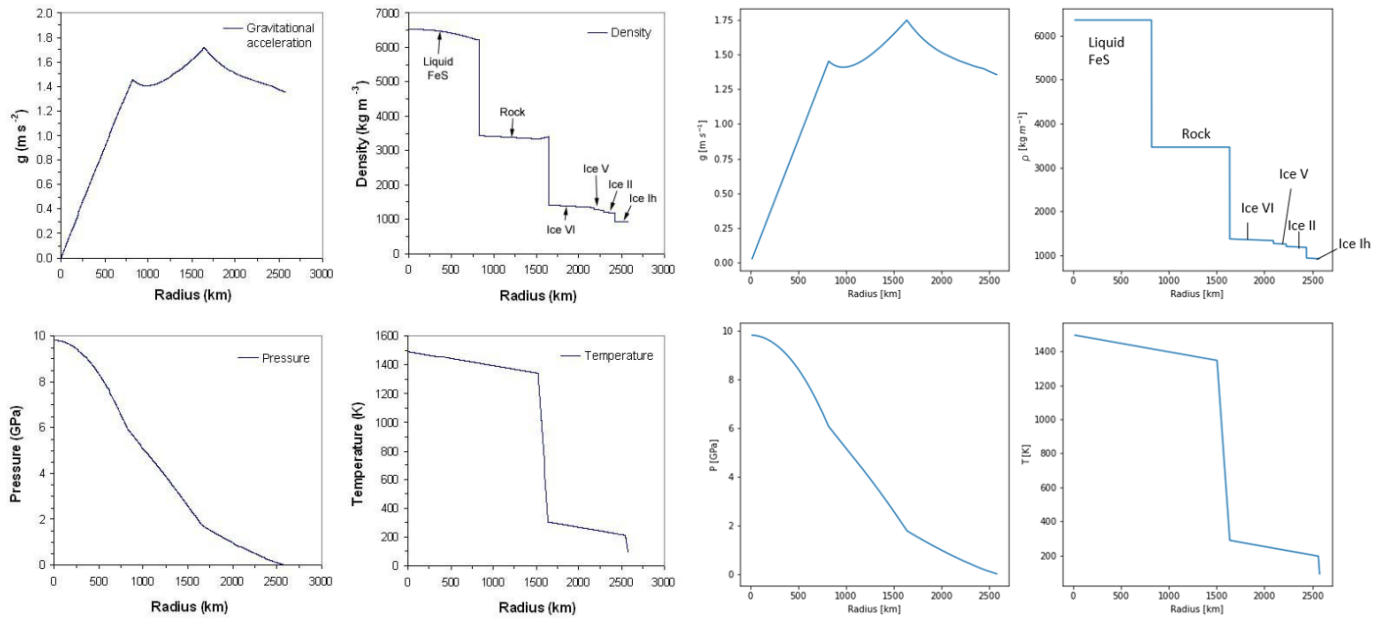

(a) Titan 'B' in Fortes (2004).

(b) Titan 'B' output.

Fig. D.2: Hydrostatic pressure profile verification.

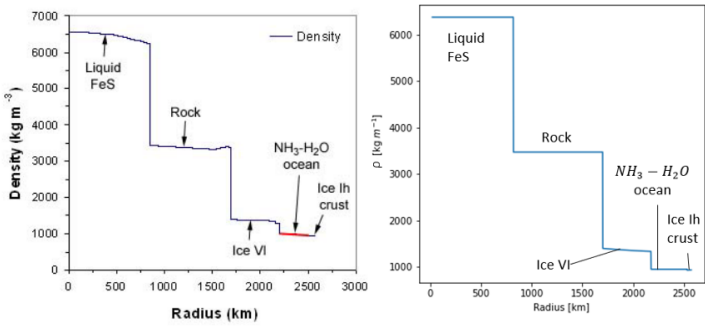

(a) Titan 'B' core with a 15wt.% NH_3 ocean in Fortes (2004).

(b) Titan 'B' core with a 15wt.% NH_3 ocean output.

Fig. D.3: Ocean profile and MoI verification.

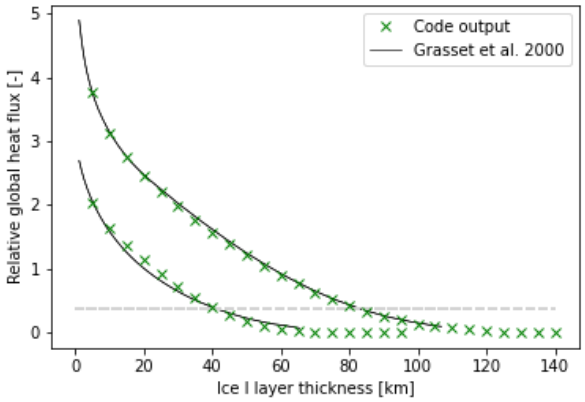

Fig. D.4: Verification of ice I shell thickness determination. Heat flux is given relative to the highest heat flux from the core (1.9 TW). Two cases are assessed: 5wt.% NH_3 (top curve) and 15wt.% NH_3 (bottom curve). The gray dashed line indicates the heat flow condition (0.7 TW). In black, results from Grasset et al. (2000).

curve), which has up to a ±3 km error in ice I layer thickness. We assess how this upper bound error propagates, and find that a thickness 40±3 km yields an ocean thickness of 399±4.2 km and a MoI of $0.32\pm7\cdot10^{-4}$. Having no impact on our findings, an error in MoI of $O(10^{-4})$ is considered negligible.

We revise our hydrostatic pressure profile by reproducing Titan 'B' in Fortes (2004). This is an ammonia-free model with ice-to-rock-to-metal ratios of 48.16:40.95:10.89. The profiles from literature are shown in Figure D.2a, and our own in Figure D.2b. In Fortes (2004), the inner FeS core extends 820 km, the olivine outer core 826 km and the ice layer 928 km. We obtain 819.76, 816.24 and 939.00 km, respectively. Owing to our assumption of constant density throughout the core, the profiles are not an exact match, but differ in the density line (top right in Figure D.2). Our model yields the same ice phases, and while the extensions of these are not provided in Fortes (2004), a visual match supports their correctness. We further verify the ice phase transition by contrasting the pressure and temperature conditions to the H_2O phase diagram, as shown in Figure D.5, and find an exact match between phase and P-T conditions.

We introduce 15wt.% ammonia in a model with the same core characteristics as Titan 'B'. In Fortes (2004), this results in an ocean extending 360 km and a MoI of 0.297. The profile is shown in Figure D.3a. In our model, shown in Figure D.3b, the ocean extends 358.60 km and the MoI is 0.297. While we expect our constant core density assumption to increase the MoI, this is not reflected in the three-decimal comparison.

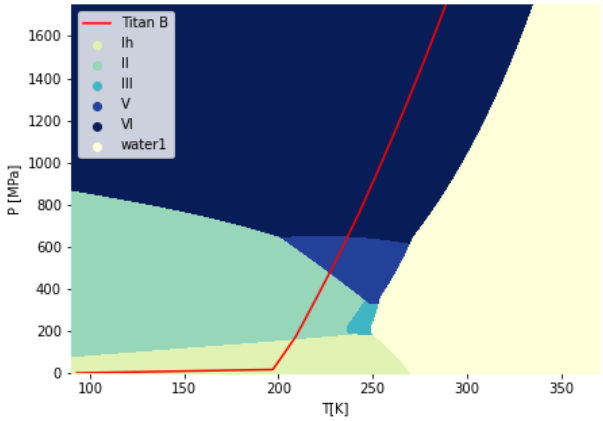

Fig. D.5: Verification of ice phase transitions for the given pressure and temperature conditions in Figure D.2b.

3

Conclusions and recommendations

This section includes the conclusions of this thesis, along with recommendations for the next steps to be followed. In chapter 2, the different methods, results and implications have been presented, with the aim of providing an overview of the research work and the derived findings.

In this thesis, Titan's birth environment has been constrained based on observations of the satellite. First, a combination of CPD characteristics has been selected, based on literature. Owing to the uncertainty in said characteristics, a selection of parameters has been examined over a wider range. The corresponding stedy-state CPDs have been modelled with ProDiMo, and the variety of chemical compositions has been studied. Secondly, we have identified the ice and NH_3 ice availability required upon Titan's formation in order to match the satellite's MoI, mean density and radius, based on a suite of interior profiles. Thirdly, we have evaluated the CPDs on their capacity to reproduce said volatile inventory. Lastly, we have assessed the implications of the obtained range of parameters and distance from Saturn that allow to form Titan with its observed characteristics.

3.1. Conclusions

Following from the research questions presented in section 1.1, and the findings described in chapter 2, a series of conclusions have been drawn and reported as answers to every question.

1. **What were the characteristics of Titan's birth environment?**

   (a) **What constraints do the observations of Titan place on its birth environment conditions?**

   We have considered a suite of interior profiles and determined how much ice and NH_3 ice should be available upon Titan's accretion, for the satellite to have a MoI of 0.33-0.34, Titan's radius and mean density. We have concluded that Titan must contain $f_{\rm ice} = 30 - 40 wt.\%$ and up to $33 wt.\%$ NH_3 ice. The CPD in which it forms can, however, contain more ice, as imperfect accretion, hydrodynamic escape, high-velocity impacts and tidal heating can lead to a decrease of up to 9% in $f_{\rm ice}$ during or after Titan's accretion. By consideration of observations of Titan, we have constrained the birth environment conditions to locations where $f_{\rm ice} = 30 - 49 wt.\%$ and up to $33 wt.\%$ NH_3 ice are available.

   (b) **What CPD characteristics are required to meet the observational constraints?**

   The MoI is more strongly dependent on the bulk ice fraction of the satellite than the NH_3 content. The ice fraction in the CPD has been found to be most sensible to the dust-to-gas ratio, out of the assessed parameters. For CPD to have $f_{\rm ice} = 30 - 49 wt.\%$, the dust-to-gas ratio must be $log(d/g) = -2.05 \pm 0.2$. Therefore, we have succeeded in placing stringent constraints on the dust-to-gas ratio that had to be present in the CPD upon Titan's accretion.

   (c) **What implications do the CPD characteristics have on the environment in which Titan formed?**

   As the dust-to-gas ratio in the solar nebula is in the order of 10^{-2} (Lodders 2003), our results indicate that no major dust filtering mechanism should be in place in Saturn's CPD,

thus supporting the absence of a gap. This is relevant in that it can be at the origin of the different architectures between the Jovian and Saturnian systems, as proposed by Sasaki et al. (2010). If Saturn did not form a gap, it is not expected to have had an inner cavity in the CPD (Sasaki et al. 2010), easing satellitesimal migration onto planet. Given the range of CPD conditions that could reproduce a satellite with Titan's characteristics in our models, Titan's origin is likely to be primordial, and, given the absence of a cavity, part of the final surviving generation in the CPD, as suggested by Charnoz et al. (2009) and Sasaki et al. (2010).

2. **What implications does the chemical composition of the CPD, as a function of radial distance to Saturn, have on the formation of a Titan-like satellite?**

   (a) **What is the closest distance to Saturn at which Titan could form?**

   Lainey et al. (2020), proposed that Titan was in very close proximity to Saturn ($\sim 5R_{\mathrm{Saturn}}$) upon gas dispersal, based on Titan's observed fast orbital migration. We have determined the closest distances to the planet at which Titan could have accreted the bulk of its mass in our CPDs. For the conditions that are expected to have been experienced by the growing satellite, the minimum radial distance for formation is $\sim 7R_{\mathrm{Saturn}}$. If Titan formed in the last generation of moons from the CPD, it could have experienced planetary luminosities as low as $L_{\mathrm{Saturn}} = 10^{-7}L_{\odot}$, for which the minimum radial distance decreases to $\sim 4R_{\mathrm{Saturn}}$. Our CPDs are therefore consistent with the formation of Titan in close proximity to the planet, although the $\sim 5R_{\mathrm{Saturn}}$ distance found by Lainey et al. (2020), requires $L_{\mathrm{Saturn}} = 10^{-7}L_{\odot}$.

   (b) **How does the chemical composition and abundance of the ices in the CPD relate to Titan's present composition?**

   Independently of where Titan formed, we find that a large NH_3 inventory was available in its building blocks, 10-20wt.% of the total nebular volatile mass from 10 to 70 R_{Saturn} for all models except when $L_{\mathrm{Saturn}} = 10^{-5}L_{\odot}$. The abundance of NH_3 in our CPDs indicates that Titan is likely to have accreted a substantial amount of this species upon formation. This supports the hypothesis the N_2 in Titan is not primordial, but proceeds from NH_3 outgassed from Titan's interior.

   (c) **What are the predictions that can be made on Titan's radial profile based on the ice and NH_3 availability upon accretion?**

   The NH_3 in Titan's interior works as an anti-freeze allowing for the presence of a subsurface ocean. In our models, the presence of 10 to 20wt.% NH_3 between 10 to 70 R_{Saturn} results in ∼300-400 km thick oceans between 53 to 28 km from the surface, respectively. These results are in agreement with the possible presence of a conductive layer at 45±15 km discovered by the Huygens probe (Béghin et al. 2010). The NH_3 abundance in our CPDs is largely insensitive to the assessed CPD conditions, ±5wt.% for 10-70 R_{Saturn}, supporting the existence of a liquid layer in Titan's interior.

   The presence of a ∼300-400 km thick ocean replaces higher density ices resulting in a low mass placement towards Titan's surface. In order to match a MoI of 0.33-0.34 with these H_2O-NH_3 solutions, the ocean density must be increased. This is possible if solutes such as magnesium sulfates or sodium sulfates are present in the liquid layer. As another option, a MoI of 0.33-0.34 can be reached if more than ∼13wt.% H_2O ice is placed in the core. Our CPD models therefore support the presence of more than 13wt.% H_2O ice in Titan's core or an ocean enriched in antifreeze compounds denser than NH_3.

3.2. Recommendations

As discussed in chapter 2, this thesis has been carried out with the intention of submitting a scientific paper on the research work in the future. Consequently, this work will be continued after the thesis defence. In this section, recommendations for future steps in the work are provided.

1. Astrochemical and interior modelling have been connected. Considering the fact that the species in the CPD do not purely translate into the chemical composition and abundances in Titan, we

propose extending the discussion on the changes that occur from the CPD to the interior. Particularly, the ice loss mechanisms should be better constrained and the evolution of the ocean thickness and composition within Titan, as found from our results, could be addressed.

2. In order to have sufficient ice in the CPD to form Titan, we found $log(d/g) = -2.05 \pm 0.2$. While $log(d/g) = [-1.85, -2.05]$ is consistent with dust-to-gas ratios in the ISM, the lower bound, $log(d/g) = -2.25$, could reflect some degree of filtering. This is a generous minimum and is not expected to reflect CPD conditions upon Titan's formation. However, the extent of filtering caused by the presence of a gap should be identified, so as to fully support (or discard) the absence of a gap in the Saturnian CPD. Towards this goal, other dust parameters should be studied: the dust minimum and maximum sizes, $a_{\min}$ and $a_{\max}$, and the powerlaw size index a_{pow}.

3. The study of the CPD's chemistry and species abundances has been focused on f_{ice}, NH_3 and H_2O+OH abundances. In future work, other species should be assessed in more detail, as these might have an effect on Titan's MoI and consequently, on where the satellite can form in the CPD. As described section 3 in the paper, CO_2 is of particular interest as it could be the source of Titan's CH_4 (Zolotov et al. 2005). Therefore, we recommend the inclusion of this species in the discussion through consideration of a gas-liquid equilibrium model of the NH_3-CO_2-H_2O system, as suggested by Marounina et al. (2018).

4. The migration of Titan, and the effect on the bulk chemistry therefrom, has been marginally considered in Appendix C: Migration. In it, migration tracks from literature have been imposed, so as to determine the effect of radial mixing in Titan's acquired bulk chemistry. This could be improved upon by both assessing a migration self-consistent with the moon's mass growth through the approach proposed in Paardekooper et al. (2010), investigating more migration tracks and performing a more in-depth literature research. These findings would help in constraining Titan's bulk composition and the maximum distance from Saturn at which it could form.

5. It is lastly recommended to indicate which future observations, experiments or studies would be most relevant to the assessment of our findings, so as to pave the road for upcoming research.

Bibliography

Anderson, J. D., Jacobson, R. A., McElrath, T. P., Moore, W. B., Schubert, G., & Thomas, P. C. (2001). Shape, mean radius, gravity field, and interior structure of Callisto. *Icarus*, *153*(1). https://doi.org/10.1006/icar.2001.6664

Anderson, J. D., Lau, E. L., Sjogren, W. L., Schubert, G., & Moore, W. B. (1996). Gravitational constraints on the internal structure of Ganymede. *Nature*, *384*(6609). https://doi.org/10.1038/384541a0

Atreya, S. K., Donahue, T. M., & Kuhn, W. R. (1978). Evolution of a nitrogen atmosphere on Titan. *Science*, *201*(4356). https://doi.org/10.1126/science.201.4356.611

Béghin, C., Sotin, C., & Hamelin, M. (2010). Titan's native ocean revealed beneath some 45km of ice by a schumann-like resonance. *Comptes Rendus Geoscience*, *342*(6), 425–433. https://doi.org/https://doi.org/10.1016/j.crte.2010.03.003

Canup, R. M. (2010). Origin of Saturns rings and inner moons by mass removal from a lost Titan-sized satellite. *Nature*. https://doi.org/10.1038/nature09661

Castillo-Rogez, J. C., & Lunine, J. I. (2010). Evolution of Titan's rocky core constrained by Cassini observations. *Geophysical Research Letters*. https://doi.org/10.1029/2010GL044398

Charnoz, S., Salmon, J., & Crida, A. (2010). The recent formation of Saturn's moonlets from viscous spreading of the main rings. *Nature*. https://doi.org/10.1038/nature09096

Charnoz, S., Crida, A., Castillo-Rogez, J. C., Lainey, V., Dones, L., Karatekin, Ö., Tobie, G., Mathis, S., Le Poncin-Lafitte, C., & Salmon, J. (2011). Accretion of Saturn's mid-sized moons during the viscous spreading of young massive rings: Solving the paradox of silicate-poor rings versus silicate-rich moons. *Icarus*. https://doi.org/10.1016/j.icarus.2011.09.017

Charnoz, S., Morbidelli, A., Dones, L., & Salmon, J. (2009). Did Saturn's rings form during the Late Heavy Bombardment? *Icarus*. https://doi.org/10.1016/j.icarus.2008.10.019

Ćuk, M., Dones, L., & Nesvorný, D. (2016). Dynamical evidence for a late formation of Saturn's moons. *The Astrophysical Journal*. https://doi.org/10.3847/0004-637x/820/2/97

Fortes, A. D. (2012). Titan's internal structure and the evolutionary consequences. *Planetary and Space Science*. https://doi.org/10.1016/j.pss.2011.04.010

Fortes, A. D., Grindrod, P. M., Trickett, S. K., & Vočadlo, L. (2007). Ammonium sulfate on Titan: Possible origin and role in cryovolcanism. *Icarus*. https://doi.org/10.1016/j.icarus.2006.11.002

Fujii, Y. I., & Ogihara, M. (2020). Formation of single-moon systems around gas giants. *Astronomy and Astrophysics*. https://doi.org/10.1051/0004-6361/201937192

Gao, P., & Stevenson, D. J. (2013). Nonhydrostatic effects and the determination of icy satellites' moment of inertia. *Icarus*. https://doi.org/10.1016/j.icarus.2013.07.034

Gautier, D., & Raulin, F. (1997). Chemical Composition of Titan's Atmosphere. In A. Wilson (Ed.), *Huygens: Science, payload and mission* (p. 359).

Grasset, O., Sotin, C., & Deschamps, F. (2000). On the internal structure and dynamics of Titan. *Planetary and Space Science*. https://doi.org/10.1016/S0032-0633(00)00039-8

Hamilton, D. P. (2013). A late major merger at Saturn: Consequences for Titan and Iapetus. *AAS/Division for Planetary Sciences Meeting Abstracts #45*, *45*, Article 302.01, 302.01.

Ida, S. (2019). The origin of Saturn's rings and moons. https://doi.org/10.1126/science.aaw3098

Iess, L., Militzer, B., Kaspi, Y., Nicholson, P., Durante, D., Racioppa, P., Anabtawi, A., Galanti, E., Hubbard, W., Mariani, M. J., Tortora, P., Wahl, S., & Zannoni, M. (2019). Measurement and implications of Saturn's gravity field and ring mass. *Science*. https://doi.org/10.1126/science.aat2965

Iess, L., Rappaport, N. J., Jacobson, R. A., Racioppa, P., Stevenson, D. J., Tortora, P., Armstrong, J. W., & Asmar, S. W. (2010). Gravity field, shape and moment of inertia of titan. *Science*. https://doi.org/10.1126/science.1182583

Jones, T. D., & Lewis, J. S. (1987). Estimated impact shock production of N2 and organic compounds on early Titan. *Icarus*, *72*(2). https://doi.org/10.1016/0019-1035(87)90181-3

Lainey, V., Casajus, L. G., Fuller, J., Zannoni, M., Tortora, P., Cooper, N., Murray, C., Modenini, D., Park, R. S., Robert, V., & Zhang, Q. (2020). Resonance locking in giant planets indicated by the rapid orbital expansion of Titan. *Nature Astronomy*. https://doi.org/10.1038/s41550-020-1120-5

Lodders, K. (2003). Solar System abundances and condensation temperatures of the elements. *The Astrophysical Journal*. https://doi.org/10.1086/375492

Lunine, J., Choukroun, M., Stevenson, D., & Tobie, G. (2010). The Origin and Evolution of Titan. *Titan from cassini-huygens*. https://doi.org/10.1007/978-1-4020-9215-2_3

Marounina, N., Grasset, O., Tobie, G., & Carpy, S. (2018). Role of the global water ocean on the evolution of Titan's primitive atmosphere. *Icarus*, *310*. https://doi.org/10.1016/j.icarus.2017.10.048

Mumma, M. J., & Charnley, S. B. (2011). The chemical composition of cometsemerging taxonomies and natal heritage. *Annual Review of Astronomy and Astrophysics*, *49*. https://doi.org/10.1146/annurev-astro-081309-130811

Niemann, H. B., Atreya, S. K., Bauer, S. J., Carignan, G. R., Demick, J. E., Frost, R. L., Gautier, D., Haberman, J. A., Harpold, D. N., Hunten, D. M., Israel, G., Lunine, J. I., Kasprzak, W. T., Owen, T. C., Paulkovich, M., Raulin, F., Raaen, E., & Way, S. H. (2005). The abundances of constituents of Titan's atmosphere from the GCMS instrument on the Huygens probe. *Nature*. https://doi.org/10.1038/nature04122

Niemann, H. B., Atreya, S. K., Demick, J. E., Gautier, D., Haberman, J. A., Harpold, D. N., Kasprzak, W. T., Lunine, J. I., Owen, T. C., & Raulin, F. (2010). Composition of Titan's lower atmosphere and simple surface volatiles as measured by the Cassini-Huygens probe gas chromatograph mass spectrometer experiment. *Journal of Geophysical Research E: Planets*. https://doi.org/10.1029/2010JE003659

Paardekooper, S. J., Baruteau, C., Crida, A., & Kley, W. (2010). A torque formula for non-isothermal type i planetary migration - I. Unsaturated horseshoe drag. *Monthly Notices of the Royal Astronomical Society*, *401*(3). https://doi.org/10.1111/j.1365-2966.2009.15782.x

Salmon, J., Charnoz, S., Crida, A., & Brahic, A. (2010). Long-term and large-scale viscous evolution of dense planetary rings. *Icarus*. https://doi.org/10.1016/j.icarus.2010.05.030

Sasaki, T., Stewart, G. R., & Ida, S. (2010). Origin of the different architectures of the jovian and saturnian satellite systems. *Astrophysical Journal*. https://doi.org/10.1088/0004-637X/714/2/1052

Tobie, G., Grasset, O., Lunine, J. I., Mocquet, A., & Sotin, C. (2005). Titan's internal structure inferred from a coupled thermal-orbital model. *Icarus*. https://doi.org/10.1016/j.icarus.2004.12.007

Tobie, G., Lunine, J., Monteux, J., Mousis, O., & Nimmo, F. (2014). The origin and evolution of Titan. *Titan: Interior, surface, atmosphere, and space environment* (pp. 29–62).

Zolotov, M., Owen, T., Atreya, S., Niemann, H., & Shock, E. (2005). An endogenic origin of titan,s methane. *AGU Fall Meeting Abstracts*, *-1*, 04.

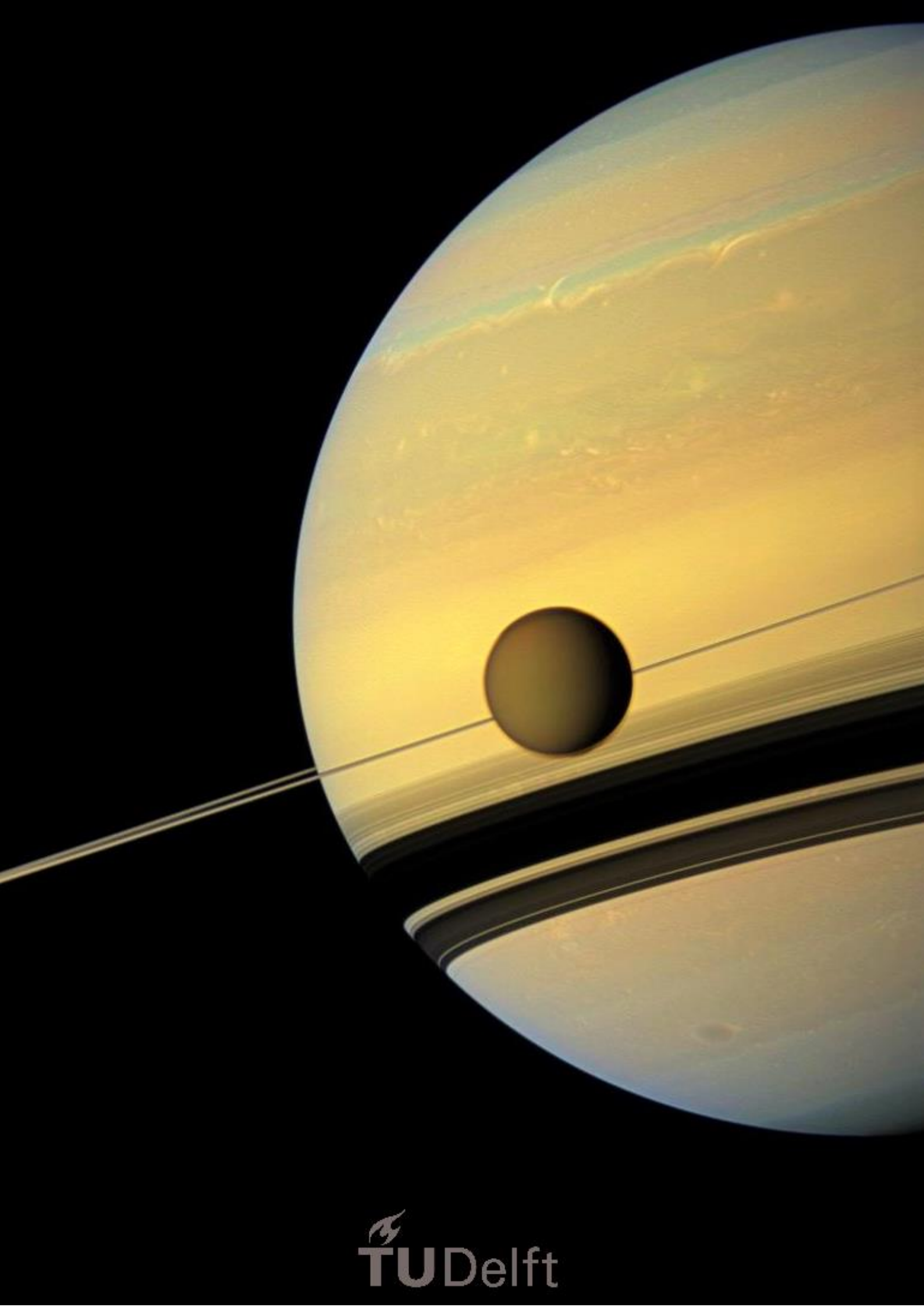
TUDelft